Late neuroprogenitors contribute to normal retinal vascular development in a *Hif2a*-dependent manner

Authors:

Enrico Cristante[1,2], Sidath E Liyanage[1,2], Robert D Sampson[1], Aikaterini Kalargyrou[1], Giulia De Rossi[3], Matteo Rizzi[1,2], Justin Hoke[1], Joana Ribeiro[1], Ryea N Maswood[1], Yanai Duran[1], Takaaki Matsuki[1], Nozie Aghaizu[1], Ulrich F Luhmann[1,2], Alexander J Smith[1], Robin R Ali[1,2], James WB Bainbridge[1,2].

Affiliations:

[1] UCL Institute of Ophthalmology, 11-43 Bath Street, London EC1V 9EL, UK

[2] NIHR Biomedical Research Centre at Moorfields Eye Hospital NHS Foundation Trust and UCL Institute of Ophthalmology, City Road, London EC1V 2PD, UK

[3] William Harvey Research Institute, Barts and the London School of Medicine and Dentistry, Queen Mary University of London, Charterhouse Square, London EC1M 6BQ, UK

Corresponding authors:

Prof James WB Bainbridge, UCL Institute of Ophthalmology, 11-43 Bath Street, London EC1V 9EL, UK j.bainbridge@ucl.ac.uk Phone: +44 (0)20 7608 6889

Dr Enrico Cristante, UCL Institute of Ophthalmology, 11-43 Bath Street, London EC1V 9EL, UK e.cristante@ucl.ac.uk Phone: +44 (0)20 7608 4053

Key words: *Hif2a*; retina; neuroprogenitor; endostatin; angiogenesis; Cre/lox

Summary statement:

Normal vascular development in the mouse retina depends on hypoxia-inducible factor 2a expression in neuroprogenitor cells.

Abstract:

In the adult central nervous system, endothelial and neuronal cells engage in tight cross-talk as key components of the so-called neurovascular unit. Impairment of their critical relationship adversely affects tissue homeostasis, as observed in neurodegenerative conditions including Alzheimer's and Parkinson's disease. In development, the influence of neuroprogenitor cells on angiogenesis is poorly understood. Here, we show that these cells interact intimately with the growing retinal vascular network, and we identify a novel regulatory mechanism of vasculature development mediated by hypoxia-inducible factor 2a (*Hif2a*). By *Cre-lox* gene excision, we show that *Hif2a* in retinal neuroprogenitor cells upregulates the expression of the pro-angiogenic mediators vascular endothelial growth factor and erythropoietin, whereas it locally downregulates the angiogenesis inhibitor endostatin. Importantly, absence of *Hif2a* in retinal neuroprogenitor cells causes a marked reduction of proliferating endothelial cells at the angiogenic front. This results in delayed retinal vascular development, fewer major retinal vessels and reduced density of the peripheral deep retinal vascular plexus. Our findings demonstrate that retinal neuroprogenitor cells are a critical component of the developing neurovascular unit.

Introduction:

Oxygen is fundamental for the development, specialization and survival of multicellular organisms (Giaccia et al., 2004). In particular, the central nervous system (CNS) is highly dependent on oxygen homeostasis for normal function and extremely vulnerable to harm from hypoxic injury. Molecular oxygen sensing mechanisms have evolved to mediate adaptive responses, including the development of new vasculature to meet the oxygen demand of developing tissues (Barneo et al., 2001; Giaccia et al., 2004). The main molecular pathway responsible for this is controlled by the basic helix-loop-helix transcription elements known as hypoxia-inducible factors (HIFs). These are heterodimers formed by an oxygen-independent β-subunit and an oxygen-dependent α-subunit, of which three variants exists: HIF1a, HIF2a (also known as EPAS1) and HIF3a (Hu et al., 2003). Hypoxic stabilization of the α-subunit enables dimerization with the β-subunit and binding of the dimer to specific sequences on gene promoters (HREs; hypoxia responsive elements) to regulate transcription and trigger responses to hypoxia including metabolic adaptation, erythropoiesis (via erythropoietin synthesis; EPO) and angiogenesis through mediators such as vascular-endothelial growth factor (VEGF) (Majmundar et al., 2010).

In the CNS, neurons (alongside glia) act as oxygen and nutrients sensors, as well as vascular regulators, by interacting structurally and functionally with blood vessels in the neurovascular unit, impairment of which plays a role in a number of neurological conditions (Hawkins and Davis, 2005). In development, neuronal networking and vascular formation go hand-in-hand, sharing common molecular cues to ensure that developing neuronal networks are supported by an appropriate vascular supply (Segura et al., 2009). The laminar development of the neuroretina and its supporting vasculature offers a valuable example and model system, in which glial and neuroretinal cells mediate a coordinated response to address increasing metabolic demand by sensing local availability of oxygen and nutrients (Fruttiger, 2007). In the mouse, astrocytes direct the formation of the superficial vascular plexus between post-natal day 1 (P1) and P8, both *via* Hif-dependent (Duan et al., 2014) and Hif-independent mechanisms (Scott et al., 2010; Weidemann et al., 2010). The metabolic demand generated in the outer plexiform layer (OPL) triggers the descent of sprouting vessels to form the deep vascular plexus (P7-P12). Vasculature

formation reaches completion and maturation by P18 with the development of the intermediate vascular plexus in the inner plexiform layer (INL) (Fruttiger, 2007). Interestingly, dividing endothelial cells do not respond to hypoxia during the process; in fact, endothelial cell-specific Hif factors are reported to be dispensable for developmental angiogenesis (Duan et al., 2014). Through this highly organized process, retinal vascular networks are structurally optimized to support one of the metabolically most demanding tissues in the body (Yu and Cringle, 2001).

Various mechanisms for the temporal and functional involvement of neuronal cells in vascular development have been proposed. Retinal ganglion cells support the astrocytes in guiding the formation of the superficial vascular plexus (Liu et al., 2013), whereas amacrine and horizontal cells guide deep and intermediate plexus formation and vasculature maturation (Usui et al., 2015) in a VEGF/Hif1a-dependent manner. Neuroprogenitor cells play a role of particular interest, since neurogenesis proceeds in parallel with angiogenesis (Hawkins and Davis, 2005). These multipotent undifferentiated cells respond to the hypoxic conditions of early neural development by self-renewing and populating the tissue (De Filippis and Delia, 2011). In anticipation of the increasing neuronal activity, neuroprogenitor cells promote vascularization and tissue oxygenation, which itself induces and supports neuronal differentiation (De Filippis and Delia, 2011).

The molecular mechanisms of this interaction between the proliferating neuroprogenitors and the developing vasculature are only partially understood. It has been previously established (Caprara et al., 2011) that Hif1a-mediated responses to hypoxia by retinal neuroprogenitor cells are involved in maintaining appropriate VEGF gradients during vascular development (Okabe et al., 2014) and in influencing the formation of the astrocytic network and the deposition of the vascular extracellular matrix (Nakamura-Ishizu et al., 2012). However, the involvement of neuroprogenitor-specific Hif2a has yet to be described, although the importance of Hif2a in vascular development is indicated by the severe retinal vasculature abnormalities observed in $Hif2a^{-/-}$ mice (Ding et al., 2005). Hif2a is structurally similar to Hif1a, but shows distinct localization and often non-redundant responses to hypoxia (Hu et al., 2003; Mowat et al., 2010), especially during development (Scortegagna et al., 2003). Hif2a is the major regulator of erythropoietin (EPO), which has powerful neuroprotective and pro-angiogenic effects in both development

and disease (Haase, 2013). Additionally, like Hif1a, Hif2a drives VEGF expression (Majmundar et al., 2010).

In the present study, we observed that *Hif2a* ablation in murine neuroprogenitor cells delayed retinal vascular development, resulting in profound abnormalities persisting into adulthood, including fewer arteries and veins, and reduced density of the deep vascular plexus peripherally. We found reduced expression of *Vegf* and *Epo* and increased levels of endostatin, known for its powerful anti-angiogenic properties in disease (Walia A et al., 2015) but not previously implicated in vascular development. Overall, our findings contribute to an understanding of the interaction between neuronal and endothelial cells, demonstrating how neuroprogenitors promote normal vascular development through the oxygen-dependent transcription factor *Hif2a*. These observations may have implications for pathological conditions in which the neurovascular cross-talk is impaired.

Results:

Hif2a is expressed in RPE, ganglion cells, astrocytes and neuroprogenitors of the post-natal developing retina

We investigated expression of *Hif2a* by immunofluorescence in retinal sections at successive postnatal time points (Fig. 1A). Nuclear expression of the protein was detected in the GCL (all ages), the retinal pigment epithelium (RPE; Fig. 1A and Fig. 1D; yellow-arrowheads), the neuroblastic layer (NBL; P0 to P6) and the INL (P9). The anatomical location of Hif2a$^+$ cells in the neuroretina suggested their ganglion cell and neuroprogenitor nature (white-arrowheads Fig. 1A), which was confirmed by co-staining with cellular markers on P3 sections: Pax6$^+$ cells in the GCL (Fig. 1B; green arrow-heads) were ganglion cells (Hitchcock et al., 1996); Pax6$^+$ cells in the NBL were neuroprogenitors (Marquardt et al., 2001) (Fig. 1B; white arrow-heads). Pdgfr-a$^+$ astrocytes instead showed only limited co-localization with Hif2a (Fig. 1C).

Cre expression and Cre-mediated recombination affects the post-natal neuroretina in the Cre^Trp1 line

Since *Hif2a* appeared to be strongly expressed in neuroprogenitors during post-natal eye development, we sought to determine its role by *Cre/lox* deletion of *Hif2a* in these cells.

The *Cre^trp1* transgenic line expresses *Cre* recombinase under the tyrosinase-related protein 1 (*Tyrp1*) promoter and has been historically employed to knock-out genes conditionally in pigmented ocular tissues such as the RPE and the iris (Mori et al., 2002). Since concerns on cell specificity were previously raised (Thanos et al., 2012) we investigated *Cre*-mediated recombination by crossing *Cre^trp1* with the reporter line *ROSA^mT/mG* (Muzumdar et al., 2007). Unexpectedly, at P1 membrane GFP (mGFP) reporter expression was evident not only in the RPE but also throughout the optic nerve and neuroretina (Fig. 2A,B). Although Cre activity appeared strongest in the peripheral retina (Fig 2A,B), significant activity was also evident in columns of cells in the central retina (Fig 2C) suggesting clonal expansion of cells resulting from Cre-mediated recombination in a common neuroprogenitor (Reese et al., 1999). Cre recombinase signal was evident on immunohistochemistry in Pax6$^+$ neuroprogenitors of the NBL (Fig. 2D), and active transcription was detected in whole neuroretina (Fig. 2E). Evidence of Cre protein in the ONL as late as P14 (Fig. 2F and Fig. S1A) indicated that *Tyrp1* promoter activity is more sustained than previously described (Mori et al., 2002).

After crossing the *Cre^Trp1* line with *Hif1a^f/f*, *Hif2a^f/f* and *Hif1a^f/f;Hif2a^f/f* lines (Gruber et al., 2006; Ryan et al., 2000), we investigated the impact of ectopic *Cre* recombinase expression by assessing the expression of *Hif* family members in P6 retinae by RT-qPCR (Fig. 2G): *Hif1a* expression was significantly reduced in *Cre^Trp1;Hif1a^f/f* and *Cre^Trp1;Hif1a^f/f;Hif2a^f/f* mice, while *Hif2a* was reduced in *Cre^Trp1;Hif2a^f/f* and *Cre^Trp1;Hif1a^f/f;Hif2a^f/f* mice.

Overall, the results indicated Cre-mediated recombination in retinal neuroprogenitors, not limited to ocular pigmented tissues as originally described (Lange et al., 2012; Mori et al., 2002).

As we previously reported a major role for Hif1a regulation on whole eye development by employing the same transgenic line (Lange et al., 2012), we compared eye size and morphology over time and observed no effect (Fig. S1B,C). Adult eyes were macroscopically normal (Fig. S1B) and showed no sign of photoreceptor (PR) degeneration (Fig. S1D,E).

$Cre^{Trp1};Hif2a^{f/f}$ and $Cre^{Trp1};Hif1a^{f/f};Hif2a^{f/f}$ mice show severely delayed developmental angiogenesis

We examined retinal vascular development at P6 (Fig. 3A and Fig. S2A) and identified a marked delay in the primary plexus formation both in $Cre^{Trp1};Hif2a^{f/f}$ and $Cre^{Trp1};Hif1a^{f/f};Hif2a^{f/f}$ in terms of both radial expansion (Fig. 3B) and vascularised area (Fig. 3C) compared with controls and Cre^{Trp1}. In both lines, fewer branch points were present in the advancing angiogenic front (Fig. 3D and Fig. S2A) and mature capillary bed (Fig. 3E and Fig. S2A). Occasionally, the forming vasculature in the $Hif2a$ KO retina showed abnormally curved arteries (Fig. S1F), reported to be a sign of vascular pathology (Han, 2012). $Hif2a$ KO lines showed no significant reduction in tip cell differentiation and/or filopodia along the angiogenic front (Fig. 3F-I), nor an increase in vascular regression, identified by empty extracellular matrix sleeves (Phng et al., 2009) (Fig. S2B,C). Since sprouting angiogenesis is typically dependent on the Notch-signalling pathway in endothelial cells (Hellström et al., 2007), we studied the expression of the major Notch receptors (Notch1 and Notch4), ligands (Dll1 and Dll4) and downstream effectors (Hes1 and Hey1) on the transcriptome of P2 FACS-sorted endothelial cells (Fig. 3J) and, in accordance with the absence of changes at the angiogenic front, we detected no significant differences in cells sorted from $Hif2a$ KO mice.

Radial progression of the primary plexus was delayed in $Hif2a$ KO lines when compared to Cre^{Trp1} and $Cre^{Trp1};Hif1a^{f/f}$, as measured centrally in terms of vascular density at P3 and P6 (Fig. 4A). Delayed angiogenesis also affected the formation of the deep and intermediate plexi (Fig. 4A, B). Hypoxic tissue between the superficial and the deficient deep plexus was detected at P9 in $Cre^{Trp1};Hif2a^{f/f}$ (Fig. 4C).

Despite delayed retinal vascular development, the hyaloid vasculature regressed almost normally in *Hif2a* KO mice: at P13, only few foetal vessels persisted, while at P18 few remnants were evident on *Cre^Trp1^;Hif2a^f/f^* and *Cre^Trp1^;Hif1a^f/f^;Hif2a^f/f^* mice (Fig. S1G).

The pigmented tissue of the iris expresses *Cre* in the *Cre^Trp1^* mouse (Lange et al., 2012; Mori et al., 2002); however, iridal vasculature developed normally in all the lines studied, with no signs of persistent pupillary membrane in adulthood (Fig. S1H).

Vascular abnormalities were still present in young adult *Hif2a* KO mice at the peripheral deep plexus level (Fig. S3B), while the remaining vasculature eventually developed a normal configuration (Fig. 4A). *Hif1a* KO lines showed a marked delay in the formation of the intermediate plexus (both centrally and peripherally) (Fig. 4A), consistent with previous observations (Caprara et al., 2011). No changes in terms of vascular permeability were observed (Fig. S1I), indicating development of an intact blood-retinal barrier.

Strikingly, *Hif2a* KO lines developed fewer arteries and veins (Fig. 4D,E) as confirmed by fluorescein angiography (Fig. S3C), together with an increased number of branch points (Fig. S3D), suggestive of a compensatory mechanism to enable fewer major vessels serve a greater portion of the tissue.

*Cre^Trp1^; Hif2a^f/f^* and *Cre^Trp1^;Hif1a^f/f^;Hif2a^f/f^* retinae show decreased endothelial proliferation, normal Vegf/Vegfr2 signalling and increased endostatin levels

At P6, the proportion of actively dividing endothelial cells at the angiogenic front (visualised by EdU incorporation) was significantly reduced in *Cre^Trp1^;Hif2a^f/f^* and *Cre^Trp1^;Hif1a^f/f^;Hif2a^f/f^* mice (Fig. 5A,B), as was the total number of endothelial cells (Fig. S4A).

Endothelial cell migration and proliferation during development are mainly driven by VEGF-A through VEGFR2 interaction on tip and stalk cells (Gerhardt et al., 2003) and decoy regulation of VEGF-A content by neural progenitors (Okabe et al., 2014). Retinae of P5 *Cre^Trp1^;Hif2a^f/f^* presented slightly reduced levels of Vegfr2 (Fig. 5C,D), possibly a consequence of the reduced endothelial cells number (Fig. S4A), but the ratio of active (phosphorylated) receptor over total Vegfr2 was unaffected (Fig. 5C-E). Although limited in its cell specificity (Stenzel et al., 2011), this whole tissue

analysis suggested that the intracellular VEGF signalling was not significantly impaired in this genotype and that factors other than VEGF-A may have been involved in driving the phenotype.

To investigate signalling molecules accounting for the delayed angiogenesis in *Hif2a KO* lines, we performed angiogenesis-specific proteome profiling of whole P6 retinal protein extracts. The most prominent change was detected for endostatin/collagen XVIII (Fig. 5F,G; red). Quantitative analysis of the 20 kDa Collagen XVIII-derived anti-angiogenic fragment endostatin (Walia A et al., 2015) by western blotting demonstrated significantly higher levels in $Cre^{Trp1};Hif2a^{f/f}$ mice (Fig. 5H,I).

Cre-mediated recombination occurs in neuroprogenitors in the Cre^{Trp1} line

To determine the extent of Cre-mediated recombination in the Cre^{Trp1} line, we performed flow cytometry on $Cre^{Trp1};ROSA^{mT/mG}$ dissociated retinae (Fig. 6A). We found that almost 50% of live retinal cells from neuroretinae of both young and adult mice were affected (Fig. 6B) (46.08±1.18% at P5; 48.57±1.40% in adults). qPCR analysis on mRNA from FACS-sorted mGFP+ cells from $Cre^{Trp1};ROSA^{mT/mG}$ and $Cre^{Trp1};Hif2a^{f/f};ROSA^{mT/mG}$ showed substantial reductions in *Hif2a* and its main transcriptionally-regulated targets, *Vegf* and *Epo* (Fig. 6C). Interestingly, few GFP+ cells could be detected in $Cre^{Trp1};ROSA^{mT/mG}$ dissociated brain tissue, whereas no GFP+ cells could be detected in spleen (Fig. S5C).

In the mouse retina, neurogenesis is characterised by two waves of cellular differentiation: the first (E11-E18) is characterised by the differentiation of early neuroprogenitors into ganglion cells, horizontal cells, cone photoreceptors, approximately half of the rod photoreceptors and a subset of amacrine cells. During the second wave (P0 to P8), remaining late neuroprogenitor cells divide asymmetrically to generate the remaining of rod photoreceptors and amacrine cells, all bipolar cells and Müller glia (Cepko, 2014). We immuno-phenotyped GFP+ cells from adult $Cre^{Trp1};ROSA^{mT/mG}$ retinae by flow cytometry (refer to Table S1, S2 and S3 and Fig. S5 for strategy and markers used). All major neuroretinal cell types showed highly similar proportions of GFP positivity at approximately 50% of the total live sub-population (Fig. 6D). Each major retinal cell type was represented within the mGFP+ sub-population similarly to whole dissociated retinae, with the exception that Müller glia cells were over-represented (Fig. 6E). This evidence suggested that Cre-

mediated recombination occurred in around 50% of an early embryonic retinal neuroprogenitor, from which late retinal neuroprogenitors and every major cell type of the neuroretina originated.

Murine retinal angiogenesis starts at P0 and late neuroprogenitor cells are known to be involved in this process (Caprara et al., 2011; Nakamura-Ishizu et al., 2012; Okabe et al., 2014). We sought to confirm whether late neuroprogenitors were affected by Cre-mediated recombination. We first assessed Pax6, a marker of neuroprogenitors (Marquardt et al., 2001) as well as ganglion cells and a fraction of amacrine cells (Hitchcock et al., 1996), and its co-localization with mGFP in P1 retina of Cre^{Trp1};$ROSA^{mT/mG}$ mice (Fig. 7A,A'). Numerous mGFP$^+$ cells appeared to ensheathe Pax6$^+$ nuclei, particularly those present in the NBL, most of which at this stage of retinal development are dividing/differentiating late neuroprogenitors (Marquardt et al., 2001; Nakamura-Ishizu et al., 2012). Quantification by flow cytometry showed that 50% of Pax6$^+$ cells stained positive for GFP in P5 Cre^{Trp1};$ROSA^{mT/mG}$ retinae (Fig. 7B,C).

To validate these findings, we crossed Cre^{Trp1} with GFP^{Rlbp1} mouse, in which post-natal GFP expression labels late neuroprogenitors (Vázquez-Chona et al., 2009). FACS-sorted GFP$^+$ cells from P5 Cre^{Trp1};GFP^{Rlbp1} showed active Cre recombinase expression (Fig. 7E), whereas P5 GFP$^+$ retinal neuroprogenitors isolated from Cre^{Trp1};$Hif2a^{f/f}$;GFP^{Rlbp1} presented significantly reduced $Hif2a$, $Vegf$ and Epo expression (Fig. 7F). These findings demonstrate the extent of Cre expression and Cre-mediated excision of floxed genes in late neuroprogenitors of Cre^{Trp1} lines.

To understand in more detail how late neuroprogenitors are structurally related to the forming vasculature, we performed iB4 staining on whole-mounted retinae of P4 wild-type GFP^{Rlbp1} mice, followed by three-dimensional rendering. Long cellular processes originated from GFP$^+$ late neuroprogenitors were visible between the NBL and the GCL, intercalating with the forming vasculature (Fig. 7G). Neuroprogenitor processes engaged in a close association with endothelial cells at the angiogenic front (red arrow-heads, Fig. 7H) as well as with post-mitotic endothelial cells in the capillary bed (Fig. 7I,J; red arrow-heads).

Retinal ganglion cells also stain positive for Pax6 (Hitchcock et al., 1996) and are key regulators of astrocytes and endothelial cells during developmental angiogenesis, through mechanisms that appear to be *Hif*-independent (Sapieha et al., 2008). We observed co-localisation of the ganglion cell marker neurofilament with GFP in *Cre^Trp1^;ROSA^mT/mG^* mice at P5 (Fig. S6A-B'). Since the arrangement of axonal extensions was similar, both centrally and peripherally (Fig. S6C), a pronounced effect on ganglion cells viability by Cre-mediated recombination and/or downregulation of *Hif* factors appears unlikely.

Other perivascular cells are affected by Cre-mediated excision but do not show strong phenotypic alterations

Retinal astrocytes play a key role in retina postnatal vascular development (Fruttiger, 2007). Unexpectedly, we found clear mGFP co-localisation with the immature astrocyte marker Pdgr-a (Fig. 8A,A') and the mature astrocyte marker Gfap (Fig. 8B) on P5 *Cre^Trp1^;ROSA^mT/mG^* eyes. By flow cytometry, we confirmed GFP and Pdgfr-a co-localisation in around 40% of astrocytes (Fig. 8C), detected active *Cre* expression in GFP⁺ astrocytes from P5 *Cre^Trp1^;ROSA^mT/mG^* mouse (Fig. 8E) and found a marked reduction in *Hif2a, Vegf* and *Epo* expression in GFP⁺ astrocytes derived from *Hif2a* KO mouse (Fig. 8F).

Although previous reports (Scott et al., 2010; Weidemann et al., 2010) found no role for astrocyte-derived Hifs or Vegf in developmental retina angiogenesis, a more recent study (Duan et al., 2014) identified the importance of astrocyte-specific Hif2a in regulating astrocyte proliferation and network formation, with consequent alterations on vascular formation. We identified in *Cre^Trp1^;Hif2a^f/f^* mice no clear morphological differences in the astrocytic network at P3 (Fig. 8G,H), consistent with a possible difference in the penetrance or efficiency of *Cre* recombinase in astrocytic lineages.

Hif1a in retinal neuroprogenitors can influence the deposition of extracellular fibronectin by retinal astrocytes (Nakamura-Ishizu et al., 2012); we identified similar defects in fibronectin deposition in *Hif1a* KO lines but no substantial difference in *Hif2a* KO mice (Fig. S7).

Pericytes participate in developmental angiogenesis and contribute to vessel stability and maturation (Bergers and Song, 2005). We detected around 20% of Ng2$^+$ pericytes to be GFP$^+$ in P5 $Cre^{Trp1};ROSA^{mT/mG}$ (Fig. S8A,B), but this did not impact on pericytes positioning around forming vasculature (Fig. S8C,D).

Resident myeloid cells (microglia) are required to promote branching patterning and tip cell filopodia formation (Fantin et al., 2010). The $Cre^{Trp1};ROSA^{mT/mG}$ mouse showed approximately 30% of CD45$^+$/CD11b$^+$ cells positive for GFP (Fig. S8E,F) but we identified no difference (Fig. S8G) at the angiogenic front of *Hif2a* KO lines.

Viral vector delivery of *Cre* recombinase to a subset of *Hif2a$^{f/f}$* late retinal neuroprogenitors recapitulates the delayed vascular development of *Hif2a* KO mice

To investigate the role of late neuroprogenitor-specific *Hif2a* in directing normal retinal vascular development, we used a recombinant adeno-associated virus (AAV) serotype 7m8 (Dalkara et al., 2013) to deliver the reporter gene *RFP* or *Cre* recombinase under the control of the neuroprogenitor-specific promoter Nestin (Tronche et al., 1999).

To target late neuroprogenitors efficiently, we injected AAV-7m8 intravitreally (Fig. S9A) soon after birth (P0.5-P1) and collected tissue at P6 (Fig. S9B). Other collection time points (P4, P18) were chosen to assess viral transduction and tropism. First, we observed Nestin-driven expression of *RFP* 3 days post-injection (P4) in cells at various levels of the NBL (Fig. 9A) with elongated morphology consistent with that of neuroprogenitors (Surzenko et al., 2013). To confirm viral tropism, *GFP^{Rlbp1}* mice were injected with AAV-Nestin.*RFP* and P4 dissociated retinae were analysed by flow cytometry. Such approach is sufficiently sensitive to assess close-to-total co-localisation of transgene (RFP) expression in GFP-expressing cells (Fig. 9B, C), supporting the high progenitors-specific tropism of this vector configuration. Nonetheless, this investigative design likely underestimates AAV-Nestin tropism and efficiency of transduction due to unavoidable experimental limitations: the relatively short time interval between AAV injection and analysis does not allow identification of all cells transduced, some of which express yet undetectable levels of fluorescent protein; the ongoing fast division of

neuroprogenitors causes dilution of the episomal AAV vector genome in daughter cells, and the Nestin promoter is inactive in neuroprogenitors differentiating into neurons or Müller glia.

The efficacy of the AAV-Nestin.*Cre* vector was validated by intravitreal administration to *ROSA^(mT/mG)* eyes, where it produced columns of GFP$^+$ cells in the ONL (Fig. S9C), reminiscent of those seen in the *Cre^(Trp1)* mouse (Fig. 5C). Sorted GFP$^+$ cells from virally injected *Hif2a^(f/f);GFP^(Rlbp1)* mice showed limited reduction in *Hif2a* expression (Fig. S9C), in accordance with the limited number of GFP$^+$ cells infected.

To determine which stage(s) of late neuroprogenitors is transduced by AAV-Nestin-vectors, we collected AAV-Nestin.*Cre*-injected *ROSA^(mT/mG)* eyes after completion of retinal development (P18) and characterised the wide-spread (Fig. 9E) GFP$^+$ population by flow cytometry and immunohistochemistry, which identified CD73$^+$ photoreceptors (43%), Müller glia (38%) and Pkc-α$^+$ rod-bipolar cells (5%; Fig. 9D and Fig. S9F-G). The absence of reliable GFP/cone arrestin co-localisation (Fig. S9H), typical morphology of rod photoreceptor cell bodies and outer segments (Fig. S9I; yellow- and white arrow-heads, respectively) and absent co-localisation of the latter with PNA-stained cone outer segments (Fig. S9J,K) confirmed rod identity of GFP$^+$ photoreceptors. We concluded that AAV-Nestin recombinant vectors injected at P0.5-P1 almost exclusively target the latest sub-class of retinal neuroprogenitors, which generates both Müller glia and a proportion of rods (Cepko, 2014). With this in mind, we investigated the effect of virally-mediated *Hif2a* ablation in these cells on retinal angiogenesis (Fig. 9E). Retinae from *Hif2a^(f/f);ROSA^(mT/mG)* mice injected with AAV-Nestin.*Cre* showed a significant reduction in radial expansion, vascularised area and branch points both at the angiogenic front and in the capillary bed (Fig. 9F,G). In addition, the number of major arteries and veins was also reduced (Fig. 9H-I). Similarly to *Cre^(Trp1);Hif2a^(f/f)* mice (Fig. 4H,I), also AAV-Nestin.*Cre*-injected *Hif2a^(f/f)* retinae showed increased levels of the anti-angiogenic peptide endostatin compared to AAV-Null-treated eyes (Fig. 9J,K).

Overall, these results closely replicate the phenotype observed in *Cre^(Trp1);Hif2a^(f/f)* and strongly support the hypothesis that late neuroprogenitor-specific *Hif2a* is a critical regulator of retinal angiogenesis/vascular development.

Since the *Cre*^{Trp1} line was originally designed to target the RPE specifically and this tissue presented strong postnatal *Hif2a* expression, we investigated the role of RPE-specific *Hif2a* on retinal angiogenesis by means of a similar viral vector approach. To target the RPE, we chose to use a recombinant HIV1-based lentiviral vector and a ubiquitous promoter (spleen focus-forming virus promoter; SFFV) (Balaggan and Ali, 2012). A single vector administration was performed subretinally into *ROSA*^{mT/mG} and *Hif2a*^{f/f}*;ROSA*^{mT/mG} mice (Fig. S10A,B). Between 20% and 40% of the RPE monolayer was transduced (Fig. S10C) and no other cell types appeared GFP$^+$ by P12 (Fig. S10D). At P6, we detected no differences in terms of radial expansion and vascularised area (Fig. S10E-G), nor of numbers of arteries and veins (Fig. S10H,I). Therefore, we concluded that RPE-specific *Hif2a* is unlikely to influence retinal vascular development.

Viral vector delivery of *Hif2a* to *Hif2a* KO late neuroprogenitor cells partially rescues the vascular phenotype

To rescue the vascular phenotype of *Hif2a* KO mice, we cloned *Hif2a* coding sequence into the AAV-Nestin vector and delivered it intravitreally to *Cre*^{Trp1}*;Hif2a*^{f/f} mice following the same experimental paradigm (Fig. S9A,B). *Hif2a* expression was significantly increased in GFP$^+$ cells sorted from P6 *Hif2a*-injected *Cre*^{Trp1}*;Hif2a*^{f/f}*;GFP*^{Rlbp1} eyes compared to Null-treated eyes (Fig. 10F). No change in radial expansion and vascularised area (Fig. 10A,B) was detected in *Cre*^{Trp1}*;Hif2a*^{f/f} mice treated with AAV-Nestin.*Hif2a*, which may depend on limitations in this experimental set-up compared to the previously described AAV-Nestin.*Cre* experiment, including: insufficient levels of *Hif2a* expression *per* cell, transient transgene expression due to cell differentiation or cell division, short treatment window. Nonetheless, *Cre*^{Trp1}*;Hif2a*^{f/f} mice treated with AAV-Nestin.*Hif2a* presented more branch points at the angiogenic front (Fig. 10C), as well as more arteries (Fig. 10D,E), and these changes were accompanied by an increase in the percentage of dividing endothelial cell nuclei (Fig. 10G,H) as well as an increase in the number of total endothelial nuclei at the angiogenic front (Fig. 10G,I). In *Cre*^{Trp1}*;Hif2a*^{f/f} mice, retinal endostatin was also significantly attenuated by AAV-Nestin.*Hif2a* administration to levels closer to those detected in *Hif2a*^{f/f} mice (Fig. 10J-K). These

findings strongly support the hypothesis that neuroprogenitor-specific *Hif2a* promotes endothelial cell division and vascular bed formation during normal development.

Discussion:

Owing to its accessible laminar anatomy and its uniquely high metabolic demand, the murine retina has been used extensively to study the consequences of neuronal hypoxia (Caprara et al., 2011; Usui et al., 2015). Historically, astrocytes have been considered the primary oxygen sentinels of the retina, however their importance is questioned by evidence of the dispensable role of the *Hif* pathway in these cells (Scott et al., 2010; Weidemann et al., 2010). Recent studies have elucidated the role played by neuronal cells as oxygen and nutrient sensors, highlighting their ability to drive and regulate physiological and pathological angiogenesis (Nakamura-Ishizu et al., 2012; Usui et al., 2015). In the current study we present evidence for a novel mechanism, centered on *Hif2a* and neuroprogenitors of the retina, which dynamically interact with the forming vasculature at the angiogenic front, promoting vascular development in an astrocyte-independent manner. Interestingly, the iridal vasculature, which is also dependent on appropriate oxygen management (Lange et al., 2012), developed normally (Fig. S1), making our findings strictly specific to retinal angiogenesis.

Initial evidence was obtained from experiments performed on the *Cre^{Trp1}* line, designed as a tool to generate efficient RPE-specific knock-outs (Mori et al., 2002). However, the promoter driving *Cre* (tyrosinase-related protein 1, an enzyme involved in pigment formation) is not RPE-specific: we have shown (Fig. 2) diffuse post-natal *Cre* expression and Cre-mediated recombination in the neuroretina, in a peripheral-to-central pattern. This is reminiscent of the *Cre^{Pax6}* line, extensively used to target neuroprogenitors and neurons in similar studies (Nakamura-Ishizu et al., 2012; Okabe et al., 2014). One possible explanation for the ectopic *Cre* recombinase expression in retinal neuroprogenitors is the involvement of the ciliary body (CB): this region hosts a pool of multipotent stem cells specialized in becoming precursors cells for retinal neurogenesis and anterior eye development (Frøen et al., 2013). Since this region of the eye shares a common developmental origin with pigmented tissues (such as the RPE and the iris pigmented epithelium), early *Tyrp1*-mediated

Cre expression may be induced in an upstream common multipotent neuroprogenitor in the *Cre^{Trp1}* mouse. Since we detected occasional cells affected by Cre-mediated excision in the brain (Fig. S5C), which also contains distinctive pigmented cells (*i.e.* the neurons in the *substantia nigra pars compacta*), this may confirm *Cre* expression as a result of the early activation of the pigment synthesis pathway. However, this does not explain why non-neuronal cells such as astrocytes, pericytes and microglia are also affected by Cre-mediated excision in this line (Fig. 8 and Fig. S8). The distinctive phagocytic abilities of these cells, their close proximity and functional interaction with developing neurons and their putative ability to undergo cell fusion/material transfer (Ogle et al., 2005) offers a plausible explanation.

Off-targeting effects in the *Cre/lox* system are well recognized, making data interpretation often difficult (Harno et al., 2013). We included the *Cre*-expressing group as a control, and confirmed our modified, neuroprogenitors-centered hypothesis through a more reliable cell-specific viral vector-based approach. The severity of the angiogenic delay observed in *Hif2a* KO lines, compared with related ones (Nakamura-Ishizu et al., 2012), was particularly pronounced (Fig. 3-4), with persistent differences in the deep vascular plexus evident to adulthood. In the wild-type neuroretina, *Hif2a* stabilization was detected until (at least) P9 in areas rich in neuroprogenitors/differentiating neurons/glia (Fig. 1), even though the on-going vascularization should have already improved the deep retinal hypoxia typical of the first week of life. This observation is consistent with the hypothesis that *Hif2a* is more susceptible to chronic (Lin et al., 2011) and subtle levels of hypoxia (Appelhoffl et al., 2004) compared with *Hif1a* and, therefore, more dynamically modulated.

Our comparison between the two main hypoxia responsive α-subunits supports a more prominent role of *Hif2a* in the developing neuroretina, consistent with the findings of previous studies (Rattner et al., 2014). Although aware of the well-described developmental role played by neuroprogenitor-specific *Hif1a* (Caprara et al., 2011), the dramatic consequences of *Hif2a* ablation were unexpected, not only in terms of temporal delay of angiogenesis and reduction in vascular complexity (Fig. 3-4), but also in terms of irreversible abnormalities such as the reduction in the number of major retinal vessels and vascular density of the intermediate plexus (Fig. 4 and Fig. S3). Similar phenotypes have been linked in previous studies to changes in

vascular regression/pruning, tip cells behavior, chemotaxis and Vegf signaling; remarkably, such parameters remained unchanged (Fig. 3 and Fig. S2B,C), as were Vegfr2 activation (Fig. 5C-E) and the expression of Notch/Dll components in endothelial cells (Fig. 3J). Instead, late retinal neuroprogenitors of the $Cre^{Trp1};Hif2a^{f/f}$ mouse showed transcriptional reduction in $Vegf$ and Epo, well known to be angio-modulatory factors. Since VEGF isoforms are the major drivers of sprouting angiogenesis (Gerhardt et al., 2003), vascular outgrowth, capillary bed complexity (Ruhrberg et al., 2002) and artery/vein patterning (Dela Paz and D'Amore, 2009), this indicates a likely mechanism of Hif2a/progenitor-dependent regulation of developmental angiogenesis. Moreover, our own findings are in close accordance with the impact of Cre^{Nestin} -mediated Vegf ablation in brain neuroprogenitors (Fantin et al., 2010), resulting in reduced vascular branching despite similar tip cell numbers. Persistent hypoxia in the neuroretina (Fig. 4) may also contribute to the defects observed in artery/vein patterning, as described in an earlier report (Claxton and Fruttiger, 2005). Epo is well recognized for both its neuroprotective and pro-angiogenic properties (Haase, 2013): although its mechanism of action has yet to be elucidated, the results of this study provide further evidence of its participation in developmental angiogenesis as previously proposed (Caprara et al., 2011).

Our experimental evidence (Figs. 5, 9, 10) suggested endostatin as another key player. This small protein fragment is derived from the proteolytic cleavage of the extracellular matrix component Collagen XVIII operated by an array of proteases including metalloproteases (MMPs) and cathepsins (Walia A et al., 2015), some of which (MMP-3 and MMP-9) are released during neurogenesis by neuroprogenitors to promote matrix remodeling and neural migration (Barkho et al., 2009). Endostatin is known for its paracrine anti-angiogenic properties, mainly exerted by blocking endothelial cells migration and proliferation via cell-cycle arrest and blockade of VEGF/VEGFR2 interaction and signaling (Walia A et al., 2015). Although well described for its role in vascular disease, evidence for its involvement in developmental angiogenesis is limited to one $in vitro$ study (Schmidt et al., 2004). We speculate that hypoxic neuroprogenitors in the avascular peripheral retina and avascular deeper cellular layers, while engaging in dynamic interactions with the forming vasculature through their cellular processes, suppress endostatin release in the vascular microenvironment to enable rapid tissue vascularisation; in addition,

they contribute to the formation of a pro-angiogenic molecular gradient ahead of the vascular front, as previously described (Gerhardt et al., 2003; Okabe et al., 2014). Once neuroprogenitors are reached by the forming vasculature and start sensing physiological oxygen level, suppression is relieved and basal levels of endostatin help stabilise and maintain mature vasculature. This hypothesis is consistent with the endogenous anti-angiogenic nature of endostatin and with the observation that mutations in *Collagen XVIII* gene that downregulate endostatin generation and/or activity predispose to the development certain tumours with a prominent vascular component (Iughetti et al., 2001).

Overall, our study describes new levels of structural and molecular association between neuronal and endothelial cells, indicating the importance of retinal neuroprogenitor/*Hif2a*-centered mechanisms in the cross-talk between neurogenesis and angiogenesis. More broadly, these findings contribute to further the understanding of neuro-vascular interactions during normal development, while modelling the pathological consequences of mis-communication at the neurovascular unit.

Materials and Methods:

Animals

All *in vivo* procedures were conducted following ethical approval of University College London and under the regulation of the UK Home Office Animals (Scientific Procedures) Act 1986. This study complied with the ARVO Statement for the Use of Animals in Ophthalmology and Vision Research. All genetic combinations were maintained on a C57BL/6J background and kept on a standard 12/12 hour light/dark cycle with food *ad libitum*. Genotyping was performed as previously described (Lange et al., 2012). The following lines were used (all under *C57Bl/6* background): transgenic mice expressing *Cre* recombinase under the control of the RPE cell-specific tyrosinase-related protein 1 promoter *Tyrp1*, referred to as Cre^{Trp1} (Lange et al., 2012; Mori et al., 2002), $Hif1a^{f/f}$ (Ryan et al., 2000), $Hif2a^{f/f}$ (Gruber et al., 2006) and combinations as reported in the Results section. Some of these combinations were crossed with $ROSA26^{mT/mG}$ (Muzumdar et al., 2007) or with GFP^{Rlbp1} (Vázquez-Chona et al., 2009). The group "controls" includes all the Cre-negative genotypes (Wild-type *C57Bl/6* and *Hif* floxed lines), as preliminary analysis revealed no

differences in basal *Hif* factors expression and comparable vasculature development.

To consistently collect pups at precise postnatal developmental stages, the morning of discovery of a new litter was designated postnatal day (P) 0. Adult mice were 4-6 weeks old.

Fluorescein and indocyanine green angiography

To analyze retinal and corneal vascular phenotype, we performed fluorescein (FA) and indocyanin green angiography (ICGA), respectively. Mice were anaesthetized by intraperitoneal injections of Dormitor (1 mg/ml; Pfizer Pharmaceuticals, UK) and ketamine (100 mg/ml; Fort Dodge Animal Health, UK) mixed with sterile water in 5:3:42 ratio. Mice were further injected intraperitoneally with 0.2 ml fluorescein (20 mg/ml) or ICG (5 mg/ml) in PBS 1X. Pupils were dilated using 1% (v/v) tropicamide and images were captured on a HRA2 scanning laser ophthalmoscope (Heidelberg Engineering, Germany) as previously described (Luhmann et al., 2009).

Intravitreal injections

Pups aged between P0.5-P1 were anaesthetized by brief ice exposure (Kim et al., 2014). Treatments were randomly assigned to left or right eyes before each litter was injected. For vasculature development experiments, one eye was injected with either AAV-7m8.Nestin.*Cre* or AAV-7m8.Nestin.*Hif2a*, whereas the contro-lateral with AAV-7m8.Null. Eye lids were incised with a 30G needle and eyes were prolapsed. Injections were performed with the aid of an operating microscope. The tip (1 mm) of a 10 mm 34-gauge needle, mounted on a 5 ml Hamilton syringe (Hamilton Bonaduz AG, Switzerland) was inserted slowly through the sclera, below the corneal limbus, until the tip of the needle was visible (bevel down) underneath the lens. 0.4 µl of vector suspension was injected carefully, monitoring eye swelling. After 10 seconds, needle was slowly withdrawn and possible reflux noted down. Pups were quickly moved to a heated mat to help post-injection recovery and then transferred back to the mother.

Evans Blue permeability assay

Evans Blue (Sigma-Aldrich, UK) was prepared (30 mg/ml) in normal saline solution (0.9% (w/v) NaCl; Sigma-Aldrich, UK) and sonicated for 5 mins. Solution was then filtered through a 5 μm filter (Millipore, UK). Mice were injected intraperitoneally at 4 ml/kg of body weight (Manaenko et al., 2011) and the dye was left circulating for 16 hours before overdosing the animal with 0.2 ml pentobarbital (intraperitoneally), collecting a sample of blood by cardiac puncture and transcardially perfusing with ice-cold PBS 1X to remove unbound dye. Eyes were enucleated, retinae dissected and wet weight calculated. Blood-retinal barrier properties were assessed by extracting and measuring bound-dye from serum and retinae as reported (Xu et al., 2001).

Preparation of flatmount samples, cryo-sections and immunofluorescence

Ocular size was assessed on freshly enucleated eyes at different time points as reported (Lange et al., 2012). Eyes were then fixed in 4% (w/v) PFA on ice for 2 hours and either dissected for RPE/choroid or retina flat-mounts as previously described (Fruttiger et al., 1996) or prepared for cryo-sectioning as described (Mowat et al., 2010).

Whole-mounts were immuno-stained as described (Pitulescu et al., 2010), whereas eye sections were immuno-stained as reported previously (Mowat et al., 2010). In both cases, primary antibody was incubated overnight at 4°C while secondary antibody was incubated for at least 2 hours at room temperature (RT); each step was followed by extensive washes. Nuclei were stained by incubation (15 mins; RT) with Hoechst 33342 (10 μM) in PBS before mounting. Nuclei rows were counted in 4 randomly selected sections/animal, both centrally and peripherally.

Vasculature and resident myeloid cells were visualized by overnight incubation at 4°C with biotin-conjugated *Bandeiraea simplicifolia* isolectin B4 (iB4; Sigma-Aldrich, UK) at 1:200 dilution, followed by Alexa 633-conjugated streptavidin incubation for 2 hours at RT. Cone outer-segments were visualized by overnight incubation at 4°C with biotin-conjugated Peanut Agglutinin (PNA; Vector Labs, UK) at 1:500 dilution, followed by Alexa 633-conjugated streptavidin incubation for 2 hours at RT.

Hypoxiprobe staining was performed as reported (Gardner et al., 2017). For three dimensional reconstructions, immunostained flatmounts were cleared before image acquisition following a published protocol (Hama et al., 2011) with modifications. Details of the antibodies used for immunohistochemistry can be found in Table S3.

Imaging and quantification

Retinal sections and flatmounts were imaged on a confocal microscope (Leica TCS SPE, Leica Microsystems, UK). Mosaic stack images were generated to visualize the entire retinal vasculature at 512 x 512 pixels resolution with a 10x dry objective, whereas higher resolution 1 μm-thick *Z*-stacks were taken at 1024 x 1024 pixels resolution with a 40x oil-immersion objective. Stacks were *Z*-projected on confocal microscope's proprietary software (Leica LAS AF). Image quantification was performed on Image J software (NIH, US); the counter was masked to the genotype and treatment received. For vascular quantification, 12 measurements of the forming vascular front (normalized to the whole retina extension) were performed and averaged for each retina sample. For characterisation of angiogenic front and capillary bed, 4 regions per retina were quantified and the mean calculated. When required, *Z*-stacks were three dimensionally reconstructed and surface rendered using Imaris software (Bitplane, Switzerland).

EdU administration and visualization

Proliferating endothelial cells at the angiogenic front were visualized by 5-ethynyl-2´-deoxyuridine (EdU) incorporation, following recommended guidelines from a commercially available kit (Click-iT EdU kit, Life-Technologies, UK).

Pups were injected intraperitoneally with 10 μl/g (body weight) 20 mM EdU solution and returned to the mother. 4 hours later pups were culled by cervical dislocation, eyes collected and fixed in 4% (w/v) PFA for 1 hour at RT. After performing standard immunofluorescence for other vascular markers, dissociated retinae were incubated in EdU reaction cocktail *as per* protocol for 30 mins at RT, protecting samples from light. After extensive washes in 0.3% (v/v) Triton X-100 PBS 1X, samples were flat-mounted and visualized by confocal microscopy.

Production of recombinant adeno-associated viral (AAV) and lentiviral particles

Cre recombinase-coding sequence was cloned into an AAV-ready pD10 backbone, into which the Nestin promoter (Lothian and Lendahl, 1997) was added or into a Lenti-ready pLenti.SFFV promoter backbone (Tschernutter et al., 2005). The red fluorescent protein (*RFP*) and the murine *Hif2a* coding sequences were obtained from a plasmid available in-house and by PCR amplification on murine retinal cDNA, respectively and cloned into the pD10.Nestin promoter backbone. Empty pD10 backbone served to produce non-expressing (Null) viral particles. The resulting constructs were used to generate AAV-7m8 recombinant particles (Dalkara et al., 2013) and VSV-G lentiviral particles as previously described (Smith et al., 2003; Tschernutter et al., 2005). AAV viral particles were purified through an AVB Sepharose column and concentrated to a final volume of 150-200 µl sterile PBS 1X using Vivaspin 4 (10 kDa) concentrators (Sartorius AG, Germany). Lentiviral particles were concentrated by ultra-centrifugation (50000 x *g*; 2.5h, 4°C) to a final volume of 200 µl sterile PBS 1X.

Tissue dissociation, immunostaining, flow cytometry sample acquisition and cell sorting

Dissected mouse retinae were dissociated into a single cell suspension for subsequent cell staining. Papain neurosphere dissociation kit (Miltenyi Biotec) was used, according to the manufacturer's instructions. Spleen and brain samples were homogenized using a 2.5 mL syringe plunger and a 70 µm filter.

Once dissociated, samples for extracellular staining (see Table S3) were spun down at 320x*g* for 5 min and stained in the dark in DMEM+ medium (supplemented with 2% FCS and 10mM HEPES) for 30 min on ice. Non-directly conjugated anti-NG2 antibody was followed by 30 mins incubation with goat anti-rabbit AF633 secondary antibody (Thermo Scientific, UK). Cells were then washed and resuspended in fresh DMEM+, filtered and stained with either SYTOX Blue (Thermo Fisher Scientific, UK) at a final concentration of 0.3 mM or DRAQ7 (Biostatus, UK) at a final concentration of 0.1 mM just before sample acquisition and/or cell sorting.

Instead, samples for intracellular staining (see Table S3) were spun down at 320x*g* for 5 min and stained in the dark with the LIVE/DEAD Fixable Violet Cell Stain (Thermo Fisher Scientific, UK) diluted in DMEM+ media for 30 min on ice. Cells were then washed with DMEM+ media and fixed in 2% PFA for 30 min on ice in the dark. Cells were washed once with 1X PBS and then resuspended in True Nuclear Transcription Factor permeabilisation buffer (BioLegend, UK) for 30 min on ice, in the dark. Cells were then washed and resuspended in neat donkey serum for 10 min. All the primary antibodies were diluted in True Nuclear permeabilisation buffer and added directly to the appropriate samples containing the donkey serum for an additional 30 min on ice, in the dark. With the exception of directly conjugated antibodies, samples were then washed with 1X PBS and resuspended in neat donkey serum for 10 min just prior to the addition of either goat anti-mouse-AF633 or goat anti-rabbit-AF633 secondary antibody (Thermo Fisher Scientific, UK) for 30 min on ice, in the dark. Samples were then washed and resuspended in 1X PBS. Please refer to Tables S1 and S3 for more detailed antibody information.

The samples were acquired using a 5-laser BD LSR Fortessa X-20 Analyser or acquired and sorted on a 5-laser BD Influx cell sorter, both equipped with 355nm (UV), 405nm (violet), 488nm (blue), 561nm (yellow) and 640nm (red) lasers. Prior to cell acquisition, samples were filtered through a 35μm cell strainer to prevent cellular aggregation.

Real-time PCR

Whole retinae were homogenized and RNA was extracted using RNeasy Mini Kit (Qiagen, UK). RNA from cells sorted into TRIzol plus (Thermo Fisher Scientific, UK) was extracted using Direct-zol microprep RNA kit (Zymo Research, USA). cDNA preparation was performed using QuantiTect Reverse Transcription Kit (Qiagen, UK) following manufacturer's instructions. Absolute and relative quantification of genes of interest was quantified by real-time probe-based PCR against endogenous *Actb* (and *Pecam-1* for sorted endothelial cells) expression levels. Real-time PCR mastermix was used *as per* recommended guidelines (Quantabio, USA). Primers were first assessed for optimal efficiency of amplification on known amounts of cDNA. Assays for *Hif1a* and *Hif2a* were designed so that the reverse primer bound within the

second exon, which is flanked by *loxP* sites in *Hif1a^f/f* and *Hif2a^f/f* lines. This allowed detection of gene knocked-out in *Cre/loxP* lines. Primers for VEGF were designed to detect all VEGF isoforms. For absolute quantification (*Hif2a*; *Cre*), in-house plasmids bearing the coding sequence of the target genes were used. Primer sequences (Thermo Scientific, UK) and probes (Roche Diagnostics, UK) are reported in Table S4.

Western Blotting

Total and phosphorylated (Y1145) VEGFR2 and endostatin levels were determined on whole retinae, snap frozen in liquid nitrogen after dissection. Tissue was lysed by repeated pipetting and following incubation for 30 mins on ice with RIPA buffer (Thermo Scientific, UK) with phosphatase (Thermo Fisher Scientific, UK) and protease inhibitor (Sigma Aldrich, UK). Equal amounts of protein were run on a reducing 4-12% gradient sodium SDS-PAGE gels (Thermo Fisher Scientific, UK). House-keeping proteins b-actin or b-tubulin were probed as loading controls. Separated proteins were electrotransferred to PVDF membranes (Millipore, UK), blocked for 1 hr at RT in 5% (w/v) BSA 0.05% (v/v) Tween-20 in PBS 1X and then incubated overnight at 4°C with primary antibodies (see Table S3). After extensive washes in 0.05% (v/v) Tween-20 PBS 1X, membranes were incubated in secondary antibodies for 2 hr at RT. Chemiluminescence detection was performed using a Fujifilm LAS-1000 Luminescence Image analyser after incubation with enhanced luminescence reagent (ECL plus; GE Healthcare, UK). Band intensities were quantified using Image J software and normalized to the house-keeping gene. For genotype comparisons, control and *KO* samples were obtained from the same litter to control for intragroup variability, whereas *Cre^Trp1* was obtained from litters of the most similar age possible. For treatment comparison, eyes were paired and compared to the Null-treated contralateral eye.

Mouse angiogenesis proteome profiler array

Retinal protein extracts (processed exactly as for Western Blot analysis) were analyzed for angiogenesis-related molecules on a proteome profiler array (R&D Systems, UK) and developed according to the manufacturer's guidelines. Images were acquired on a Nikon LAS4000 CCD imager and densitometry was performed

with ImageJ. Membranes were normalized to each other using positive control spots and background reading (Chu et al., 2016).

Statistical analysis

Data are presented as mean±s.e.m and sample sizes are reported in each figure legend. Each experiment on animals was performed at least on 2 independent litters of a given genotype. Data were plotted and analyzed for statistical significance using Graphpad Prism software (Graphpad Software Inc., USA). First, normal distribution was assessed for each group by Kolmogorov-Smirnov test. Parametric statistical tests (two-tailed *t*-test and one- or two-way ANOVA) were used to compare between averages of two or more groups, with *post-hoc* Tukey's or Bonferroni's multiple comparison test. *P* values less than 0.05 were considered statistically significant.

Author contributions:

Conception, design and execution of experiments: EC, SEL, RDS, AK, GDR, MR, JH, YD, JR, RNM, AJS. Sharing protocols and reagents: TM, NA. Analysis and interpretation: EC, SEL, RDS, MR, UFL, AJS, JWB. Drafting the article: EC. Critical revision of the article: SEL, GDR, AJS, RRA, JWB. Funding: RRA, JWB. The manuscript was finally approved by all authors.

Funding:

References:

Appelhoffl, R. J., Tian, Y. M., Raval, R. R., Turley, H., Harris, A. L., Pugh, C. W., Ratcliffe, P. J. and Gleadle, J. M. (2004). Differential function of the prolyl hydroxylases PHD1, PHD2, and PHD3 in the regulation of hypoxia-inducible factor. *J. Biol. Chem.* **279**, 38458–38465.

Balaggan, K. S. and Ali, R. R. (2012). Ocular gene delivery using lentiviral vectors. *Gene Ther.* **19**, 145–53.

Barkho, B., Munoz, A., Li, X., Li, L., Cunningham, A. and Zhao, X. (2009). Endogenous Matrix Metalloproteinase (MMP)-3 and MMP-9 Promote the Differentiation and Migration of Adult Neural Progenitor Cells in Response to Chemokines. *Stem Cells* **26**, 3139–3149.

Barneo, J., Pardal, R. and P, O.-S. (2001). Cellular mechanism of oxygen sensing. *Annu. Rev. Physiol.* **63**, 259–87.

Bergers, G. and Song, S. (2005). The role of pericytes in blood-vessel formation and maintenance. *Neuro. Oncol.* **7**, 452–464.

Caprara, C., Thiersch, M., Lange, C., Joly, S., Samardzija, M. and Grimm, C. (2011). HIF1A is essential for the development of the intermediate plexus of the retinal vasculature. *Investig. Ophthalmol. Vis. Sci.* **52**, 2109–2117.

Cepko, C. (2014). Intrinsically different retinal progenitor cells produce specific types of progeny. *Nat. Rev. Neurosci.* **15**, 615–627.

Chu, C. J., Gardner, P. J., Copland, D. A., Liyanage, S. E., Gonzalez-Cordero, A., Kleine Holthaus, S.-M., Luhmann, U. F. O., Smith, A. J., Ali, R. R. and Dick, A. D. (2016). Multimodal analysis of ocular inflammation using the endotoxin- induced uveitis mouse model. *Dis. Model. Mech.* **9**, 473–481.

Claxton, S. and Fruttiger, M. (2005). Oxygen modifies artery differentiation and network morphogenesis in the retinal vasculature. *Dev. Dyn.* **233**, 822–828.

Dalkara, D., Byrne, L. C., Klimczak, R. R., Visel, M., Yin, L., Merigan, W. H., Flannery, J. G. and Schaffer, D. V (2013). In vivo-directed evolution of a new adeno-associated virus for therapeutic outer retinal gene delivery from the vitreous. *Sci. Transl. Med.* **5**, 1–11.

De Filippis, L. and Delia, D. (2011). Hypoxia in the regulation of neural stem cells. *Cell. Mol. Life Sci.* **68**, 2831–2844.

Dela Paz, N. G. and D'Amore, P. A. (2009). Arterial versus venous endothelial cells. *Cell Tissue Res.* **335**, 5–16.

Ding, K., Scortegagna, M., Seaman, R., Birch, D. G. and Garcia, J. A. (2005). Retinal disease in mice lacking hypoxia-inducible transcription factor-2a. *Investig. Ophthalmol. Vis. Sci.* **46**, 1010–1016.

Duan, L. J., Takeda, K. and Fong, G. H. (2014). Hypoxia inducible factor-2a regulates the development of retinal astrocytic network by maintaining adequate supply of astrocyte progenitors. *PLoS One* **9**, 1–12.

Fantin, A., Vieira, J. M., Gestri, G., Denti, L., Schwarz, Q., Prykhozhij, S., Peri, F., Wilson, S. W. and Ruhrberg, C. (2010). Tissue macrophages act as cellular chaperones for vascular anastomosis downstream of VEGF-mediated endothelial tip cell induction. *Blood* **116**, 829–840.

Frøen, R., Johnsen, E. O., Nicolaissen, B., Facskó, A., Petrovski, G. and Moe, M. C. (2013). Does the adult human ciliary body epithelium contain "true" retinal stem cells? *Biomed Res. Int.* **2013**, 1–7.

Fruttiger, M. (2007). Development of the retinal vasculature. *Angiogenesis* **10**, 77–88.

Fruttiger, M., Calver, A. R., Kru, W. H., Mudhar, H. S., Michalovich, D., Takakura, N., Nishikawa, S. I. and Richardson, W. D. (1996). PDGF Mediates a Neuron – Astrocyte Interaction in the Developing Retina. *Neuron* **17**, 1117–1131.

Gardner, P. J., Liyanage, S. E., Cristante, E., Sampson, R. D., Dick, A. D., Ali, R. R. and Bainbridge, J. W. (2017). Hypoxia inducible factors are dispensable for myeloid cell migration into the inflamed mouse eye. *Sci. Rep.* **7**, 40830.

Gerhardt, H., Golding, M., Fruttiger, M., Ruhrberg, C., Lundkvist, A., Abramsson, A., Jeltsch, M., Mitchell, C., Alitalo, K., Shima, D., et al. (2003). VEGF guides angiogenic sprouting utilizing endothelial tip cell filopodia. *J. Cell Biol.* **161**, 1163–1177.

Giaccia, A. J., Simon, M. C. and Johnson, R. (2004). The biology of hypoxia: the

role of oxygen sensing in development, normal function, and disease. *Genes Dev.* **18**, 2183–2194.

Grossman, R., Fox, L. E., Gorovits, R., Ben-Dror, I., Reisfeld, S. and Vardimon, L. (1994). Molecular basis for differential expression of glutamine synthetase in retina glia and neurons. *Mol. Brain Res.* **21**, 312–320.

Gruber, M., Hu, C., Johnson, R. S., Brown, E. J., Keith, B. and Simon, M. C. (2006). Acute postnatal ablation of Hif-2a results in anemia. *Proc. Natl. Acad. Sci. U. S. A.* **104**, 2301–2306.

Haase, V. H. (2013). Regulation of erythropoiesis by hypoxia-inducible factors. *Blood Rev.* **27**, 41–53.

Hama, H., Kurokawa, H., Kawano, H., Ando, R., Shimogori, T., Noda, H., Fukami, K., Sakaue-sawano, A. and Miyawaki, A. (2011). Sca l e : a chemical approach for fluorescence imaging and reconstruction of transparent mouse brain. *Nat. Neurosci.* **14**, 1481–1488.

Han, H. (2012). Twisted Blood Vessels : Symptoms , Etiology and Biomechanical Mechanisms. *J. Vasc. Res.* **49**, 185–197.

Harno, E., Cottrell, E. C. and White, A. (2013). Metabolic pitfalls of CNS cre-based technology. *Cell Metab.* **18**, 21–28.

Hawkins, B. T. and Davis, T. P. (2005). The Blood-Brain Barrier / Neurovascular Unit in Health and Disease. *Pharmacol. Rev.* **57**, 173–185.

Hellström, M., Phng, L., Hofmann, J. J., Wallgard, E., Coultas, L., Lindblom, P., Alva, J., Nilsson, A.-K., Karlsson, L., Gaiano, N., et al. (2007). Dll4 signalling through Notch1 regulates formation of tip cells during angiogenesis. *Nature* **445**, 776–780.

Hitchcock, P., Macdonald, R., VanDeRyt, J. and Wilson, S. (1996). Antibodies against Pax6 immunostain amacrine and ganglion cells and neuronal progenitors, but not rod precursors, in the normal and regenerating retina of the goldfish. *J Neurobiol* **29**, 399–413.

Hu, C., Wang, L., Chodosh, L. a, Keith, B. and Simon, M. C. (2003). Differential Roles of Hypoxia-Inducible Factor 1 alpha (HIF-1 alpha) and HIF-2 alpha in

Hypoxic Gene Regulation. *Mol. Cell. Biol.* **23**, 9361–9374.

Iughetti, P., Suzuki, O., Godoi, P. H. C., Alves, V. A. F., Sertié, A. L., Zorick, T., Soares, F., Camargo, A., Moreira, E. S., Di Loreto, C., et al. (2001). A polymorphism in endostatin, an angiogenesis inhibitor, predisposes for the development of prostatic adenocarcinoma. *Cancer Res.* **61**, 7375–7378.

Jeon, C.-J., Strettoi, E. and Masland, R. H. (1998). The major cell populations of the mouse retina. *J. Neurosci.* **18**, 8936–46.

Kim, J.-Y., Grunke, S. D., Levites, Y., Golde, T. E. and Jankowsky, J. L. (2014). Intracerebroventricular viral injection of the neonatal mouse brain for persistent and widespread neuronal transduction. *J. Vis. Exp.* **91**, 51863–51873.

Koso, H., Minami, C., Tabata, Y., Inoue, M., Sasaki, E., Satoh, S. and Watanabe, S. (2009). CD73, a novel cell surface antigen that characterizes retinal photoreceptor precursor cells. *Investig. Ophthalmol. Vis. Sci.* **50**, 5411–5418.

Lange, C. a K., Luhmann, U. F. O., Mowat, F. M., Georgiadis, A., West, E. L., Abrahams, S., Sayed, H., Powner, M. B., Fruttiger, M., Smith, A. J., et al. (2012). Von Hippel-Lindau protein in the RPE is essential for normal ocular growth and vascular development. *Development* **139**, 2340–50.

Lin, Q., Cong, X. and Yun, Z. (2011). Differential Hypoxic Regulation of Hypoxia-Inducible Factors 1 and 2. *Mol. Cancer Res.* **9**, 757–765.

Liu, H., Kim, S.-Y., Fu, Y., Wu, X., Ng, L., Swaroop, A. and Forrest, D. (2013). An isoform of retinoid-related orphan receptor β directs differentiation of retinal amacrine and horizontal interneurons. *Nat. Commun.* **4**, 1813.

Liyanage, S. E., Fantin, A., Villacampa, P., Lange, C. A., Denti, L., Cristante, E., Smith, A. J., Ali, R. R., Luhmann, U. F., Bainbridge, J. W., et al. (2016). Myeloid-Derived Vascular Endothelial Growth Factor and Hypoxia-Inducible Factor Are Dispensable for Ocular Neovascularization-Brief Report. *Arterioscler. Thromb. Vasc. Biol.* **36**,.

Lothian, C. and Lendahl, U. (1997). An Evolutionarily Conserved Region in the Second Intron of the Human Nestin Gene Directs Gene Exmession to CNS Progenitor Cells and to Early Neural Crest Cells. *Eur. J. Neurosci.* **9**, 452–462.

Luhmann, U. F. O., Robbie, S., Munro, P. M. G., Barker, S. E., Duran, Y., Luong, V., Fitzke, F. W., Bainbridge, J. W. B., Ali, R. R. and Maclaren, R. E. (2009). The drusenlike phenotype in aging Ccl2-knockout mice is caused by an accelerated accumulation of swollen autofluorescent subretinal macrophages. *Investig. Ophthalmol. Vis. Sci.* **50**, 5934–5943.

Macosko, E. Z., Basu, A., Satija, R., Nemesh, J., Shekhar, K., Goldman, M., Tirosh, I., Bialas, A. R., Kamitaki, N., Martersteck, E. M., et al. (2015). Highly parallel genome-wide expression profiling of individual cells using nanoliter droplets. *Cell* **161**, 1202–1214.

Majmundar, A. J., Wong, W. J. and Simon, M. C. (2010). Hypoxia-inducible factors and the response to hypoxic stress. *Mol Cell* **40**, 294–309.

Manaenko, A., Chen, H., Kammer, J., Zhang, J. H. and Tang, J. (2011). Comparison Evans Blue injection routes: Intravenous versus intraperitoneal, for measurement of blood-brain barrier in a mice hemorrhage model. *J. Neurosci. Methods* **195**, 206–210.

Marquardt, T., Ashery-padan, R., Andrejewski, N., Scardigli, R., Guillemot, F. and Gruss, P. (2001). Pax6 Is Required for the Multipotent State of Retinal Progenitor Cells. *Cell* **105**, 43–55.

Mori, M., Metzger, D., Garnier, J., Chambon, P. and Mark, M. (2002). Site-Specific Somatic Mutagenesis in the Retinal Pigment Epithelium. *Investig. Ophthalmol. Vis. Sci.* **43**, 1384–1388.

Mowat, F. M., Luhmann, U. F. O., Smith, A. J., Lange, C., Duran, Y., Harten, S., Shukla, D., Maxwell, P. H., Ali, R. R. and Bainbridge, J. W. B. (2010). HIF-1alpha and HIF-2alpha are differentially activated in distinct cell populations in retinal ischaemia. *PLoS One* **5**, 1–9.

Muzumdar, M., Tasic, B., Miyamichi, K., Li, L. and Luo, L. (2007). A global double-fluorescent Cre reporter mouse. *Genesis* **45**, 418–426.

Nakamura-Ishizu, A., Kurihara, T., Okuno, Y., Ozawa, Y., Kishi, K., Goda, N., Tsubota, K., Okano, H., Suda, T. and Kubota, Y. (2012). The formation of an angiogenic astrocyte template is regulated by the neuroretina in a HIF-1-

dependent manner. *Dev. Biol.* **363**, 106–114.

Ogle, B. M., Cascalho, M. and Platt, J. L. (2005). Biological implications of cell fusion. *Nat. Rev. Mol. Cell Biol.* **6**, 567–575.

Okabe, K., Kobayashi, S., Yamada, T., Kurihara, T., Tai-Nagara, I., Miyamoto, T., Mukouyama, Y. S., Sato, T. N., Suda, T., Ema, M., et al. (2014). Neurons limit angiogenesis by titrating VEGF in retina. *Cell* **159**, 584–596.

Ozerdem, U., Grako, K. A., Dahlin-Huppe, K., Monosov, E. and Stallcup, W. B. (2001). NG2 proteoglycan is expressed exclusively by mural cells during vascular morphogenesis. *Dev. Dyn.* **222**, 218–227.

Phng, L., Potente, M., Leslie, J. D., Babbage, J., Nyqvist, D., Lobov, I., Ondr, J. K., Rao, S., Lang, R. A., Thurston, G., et al. (2009). Nrarp Coordinates Endothelial Notch and Wnt Signaling to Control Vessel Density in Angiogenesis. *Dev. Cell* **16**, 70–82.

Pitulescu, M. E., Schmidt, I., Benedito, R. and Adams, R. H. (2010). Inducible gene targeting in the neonatal vasculature and analysis of retinal angiogenesis in mice. *Nat. Protoc.* **5**, 1518–1534.

Rattner, A., Wang, Y., Zhou, Y., Williams, J. and Nathans, J. (2014). The role of the hypoxia response in shaping retinal vascular development in the absence of norrin/frizzled4 signaling. *Investig. Ophthalmol. Vis. Sci.* **55**, 8614–8625.

Reese, B. E., Necessary, B. D., Tam, P. P. L., Faulkner-Jones, B. and Tan, S. S. (1999). Clonal expansion and cell dispersion in the developing mouse retina. *Eur. J. Neurosci.* **11**, 2965–2978.

Ruether, K., Feigenspan, A., Pirngruber, J., Leitges, M., Baehr, W. and Strauss, O. (2010). Pkc-a is essential for the proper activation and termination of rod bipolar cell response. *Investig. Ophthalmol. Vis. Sci.* **51**, 6051–6058.

Ruhrberg, C., Gerhardt, H., Golding, M., Watson, R., Ioannidou, S., Fujisawa, H., Betsholtz, C. and Shima, D. T. (2002). Spatially restricted patterning cues provided by heparin-binding VEGF-A control blood vessel branching morphogenesis. *Genes Dev.* **16**, 2684–2698.

Ryan, H. E., Poloni, M., Mcnulty, W., Elson, D., Gassmann, M., Arbeit, J. M. and

Johnson, R. S. (2000). Advances in Brief Hypoxia-inducible Factor-1 α Is a Positive Factor in Solid Tumor Growth. *Cancer Res.* **60**, 4010–4015.

Sapieha, P., Sirinyan, M., Hamel, D., Zaniolo, K., Joyal, J.-S., Cho, J.-H., Honoré, J.-C., Kermorvant-Duchemin, E., Varma, D. R., Tremblay, S., et al. (2008). The succinate receptor GPR91 in neurons has a major role in retinal angiogenesis. *Nat. Med.* **14**, 1067–1076.

Schmidt, A., Wenzel, D., Ferring, I., Kazemi, S., Sasaki, T., Timpl, R., Addicks, K., Fleischmann, B. K. and Bloch, W. (2004). Influence of Endostatin on Embryonic Vasculo- and Angiogenesis. 468–480.

Scortegagna, M., Ding, K., Oktay, Y., Gaur, A., Thurmond, F., Yan, L.-J., Marck, B. T., Matsumoto, A. M., Shelton, J. M., Richardson, J. a, et al. (2003). Multiple organ pathology, metabolic abnormalities and impaired homeostasis of reactive oxygen species in Epas1-/- mice. *Nat. Genet.* **35**, 331–340.

Scott, A., Powner, M. B., Gandhi, P., Clarkin, C., Gutmann, D. H., Johnson, R. S., Ferrara, N. and Fruttiger, M. (2010). Astrocyte-derived vascular endothelial growth factor stabilizes vessels in the developing retinal vasculature. *PLoS One* **5**, 1–7.

Segura, I., De Smet, F., Hohensinner, P. J., Almodovar, C. R. de and Carmeliet, P. (2009). The neurovascular link in health and disease: an update. *Trends Mol. Med.* **15**, 439–451.

Smith, A. J., Schlichtenbrede, F. C., Tschernutter, M., Bainbridge, J. W., Thrasher, A. J. and Ali, R. R. (2003). AAV-mediated gene transfer slows photoreceptor loss in the RCS rat model of retinitis pigmentosa. *Mol. Ther.* **8**, 188–195.

Stanescu-Segall, D., Birke, K., Wenzel, A., Grimm, C., Orgul, S., Fischer, J. A., Born, W. and Hafezi, F. (2015). PAX6 Expression and Retinal Cell Death in a Transgenic Mouse Model for Acute Angle-Closure Glaucoma. *J. Glaucoma* **24**, 426–32.

Stenzel, D., Lundkvist, a., Sauvaget, D., Busse, M., Graupera, M., van der Flier, a., Wijelath, E. S., Murray, J., Sobel, M., Costell, M., et al. (2011). Integrin-

dependent and -independent functions of astrocytic fibronectin in retinal angiogenesis. *Development* **138**, 4451–4463.

Surzenko, N., Crowl, T., Bachleda, A., Langer, L. and Pevny, L. (2013). SOX2 maintains the quiescent progenitor cell state of postnatal retinal Muller glia. *Development* **140**, 1445–56.

Tao, C. and Zhang, X. (2014). Development of astrocytes in the vertebrate eye. *Dev. Dyn.* **243**, 1501–1510.

Thanos, A., Morizane, Y., Murakami, Y., Giani, A., Mantopoulos, D., Kayama, M., Roh, M. I., Michaud, N., Pawlyk, B., Sandberg, M., et al. (2012). Evidence for baseline retinal pigment epithelium pathology in the Trp1-Cre mouse. *Am. J. Pathol.* **180**, 1917–1927.

Tronche, F., Kellendonk, C., Kretz, O., Gass, P., Anlag, K., Orban, P. C., Bock, R., Klein, R. and Schutz, G. (1999). Disruption of the glucocorticoid receptor gene in the nervous system results in reduced anxiety. *Nat. Genet.* **23**, 99–103.

Tschernutter, M., Schlichtenbrede, F. C., Howe, S., Balaggan, K. S., Munro, P. M., Bainbridge, J. W. B., Thrasher, A. J., Smith, A. J. and Ali, R. R. (2005). Long-term preservation of retinal function in the RCS rat model of retinitis pigmentosa following lentivirus-mediated gene therapy. *Gene Ther.* **12**, 694–701.

Usui, Y., Westenskow, P. D., Kurihara, T., Aguilar, E., Sakimoto, S., Paris, L. P., Wittgrove, C., Feitelberg, D., Friedlander, M. S. H., Moreno, S. K., et al. (2015). Neurovascular crosstalk between interneurons and capillaries is required for vision. *J. Clin. Invest.* **125**, 2335–2346.

Vázquez-Chona, F., Clark, A. M. and Levine, E. M. (2009). Rlbp1 promoter drives robust Muller glial GFP expression in transgenic mice. *Investig. Ophthalmol. Vis. Sci.* **50**, 3996–4003.

Walia A, Yang, J., Huang, Y., Rosenblatt, M., Chang, J. and Azar, D. (2015). Endostatin's emerging roles in angiogenesis, lymphangiogenesis, disease, and clinical applications. *Proc. Natl. Acad. Sci. U. S. A.* **1850**, 2422–2438.

Weidemann, A., Krohne, T. U., Aguilar, E., Kurihara, T., Dorrell, M. I., Simon, M.

C., Haase, V. H., Friedlander, M. and Johnson, R. S. (2010). Astrocyte hypoxic response is essential for pathological but not developmental angiogenesis of the retina. *Glia* **58**, 1177–1185.

Xu, Q., Qaum, T. and Adamis, A. P. (2001). Sensitive Blood – Retinal Barrier Breakdown Quantitation using Evans Blue. *Invest. Ophthalmol. Vis. Sci.* **42**, 789–794.

Yu, D. Y. and Cringle, S. J. (2001). Oxygen distribution and consumption within the retina in vascularised and avascular retinas and in animal models of retinal disease. *Prog. Retin. Eye Res.* **20**, 175–208.

Figures
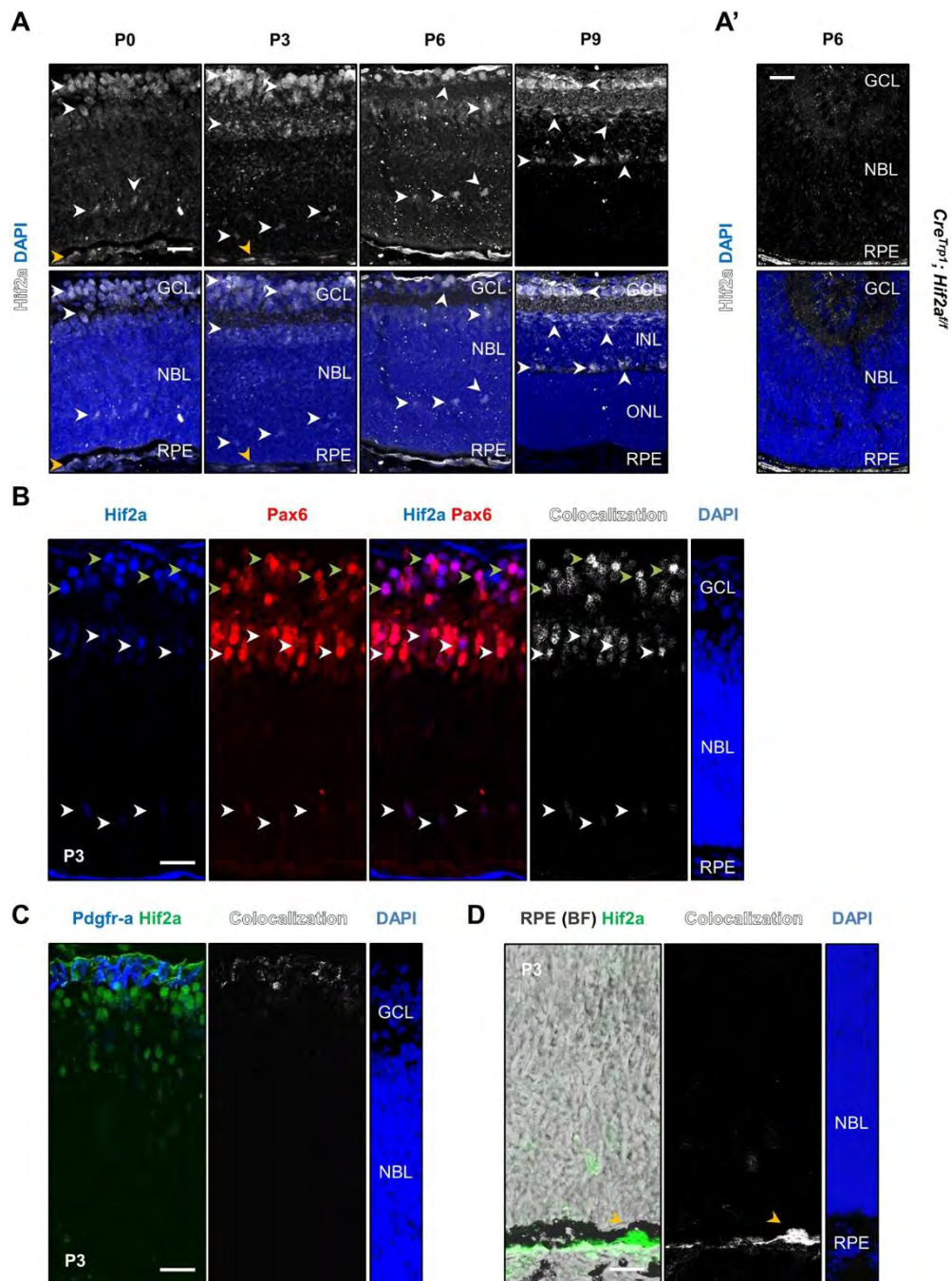
Fig. 1: Expression of *Hif2a* in the eye after birth. (A) Hif2a staining was detected in cell nuclei in the GCL at all ages analysed, in the NBL at P0, P3 and P6 and in the INL at P9 (white arrow-heads), as well as RPE nuclei (orange arrow-heads). (A') Absence of specific Hif2a signal in P6 *Cre^{Trp1}; Hif2a^{f/f}* tissue. (B) Co-labelling of Hif2a and Pax6 in retinal ganglion cells (see green arrow-heads) and neuroprogenitors

(various locations of the NBL; see white arrow-heads). (C) Co-staining with Pdgfr-a in astrocytes. Panel (D) shows Hif2a in the RPE, visualised on bright-field (BF) through its pigmentation (orange arrow-heads). Scale bars: 25µm in (A-D).
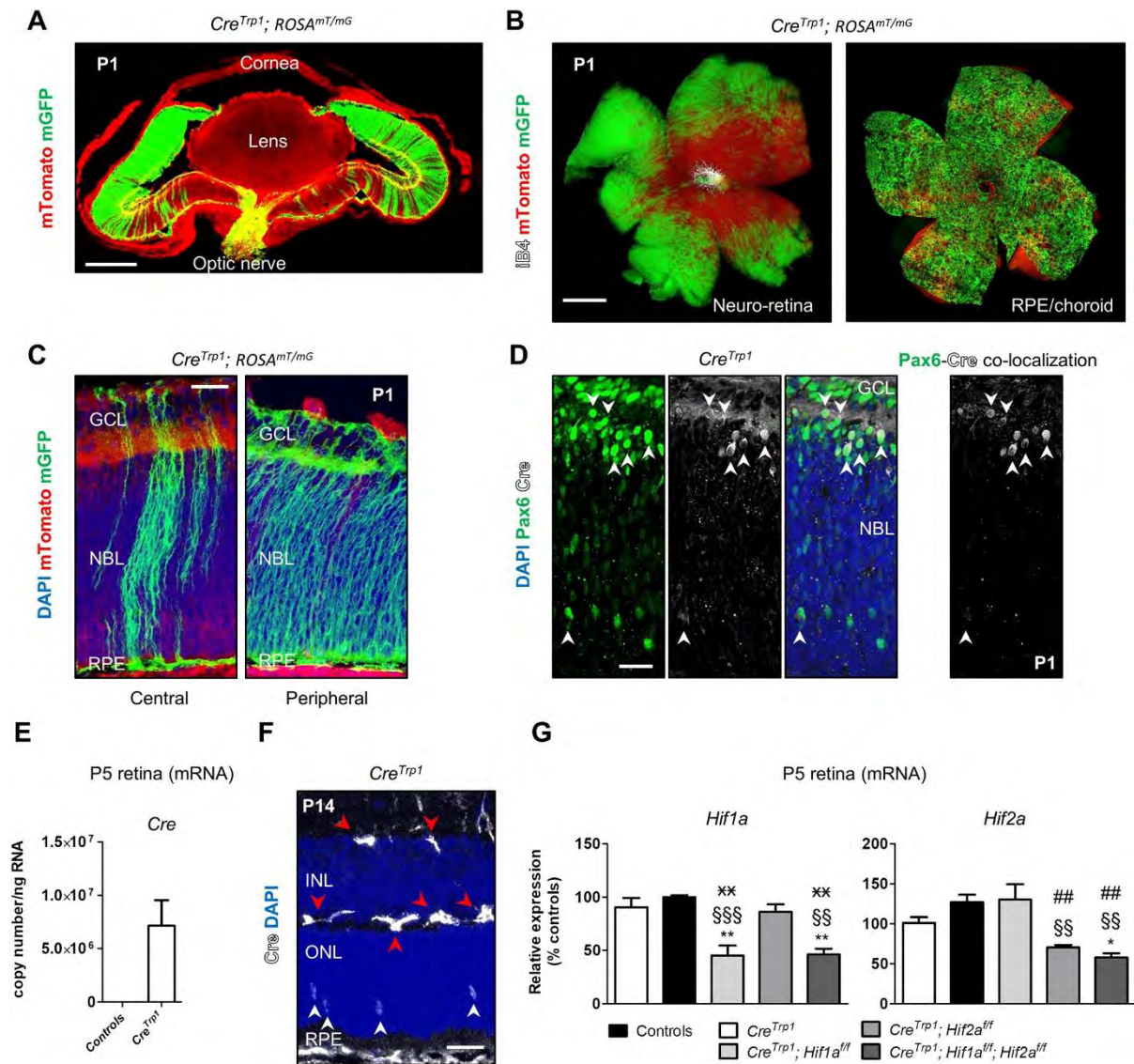
Fig. 2: *Cre* expression is not limited to RPE in the *Cre^Trp1^* line. (A) Whole eye section from a P1 *Cre^Trp1^* crossed with *ROSA^mT/mG^* line. Membrane-localized GFP expression present throughout the whole neuroretina, particularly in the peripheral region. (B) Retinal and choroid/RPE flatmounts of *Cre^Trp1^;ROSA^mT/mG^* P1 eye showing peripheral GFP expression in the retina and RPE. (C) High-magnification of central and peripheral regions (age: P1); GFP+ cells are organised in columns, reminiscent of developmental clonal expansion. (D) Pax6 and Cre staining of P1 eye section (co-staining highlighted by white-arrowheads). (E) RT-qPCR analysis of *Cre* in P5 whole retinae mRNA extracts. n=5. (F) Cre staining of a P14 eye section (highlighted by white-arrowheads). Non-specific binding of secondary antibody to blood vessels (red-arrowheads; also refer to Fig. S1A). (G) RT-qPCR analysis of *Hif1a* and *Hif2a* in whole retina RNA extracts (age: P6). Values are relative

percentages of the controls (n=5-8). ANOVA and Tukey's multiple comparison test: *P<0.05, **P<0.01 vs. controls; §§P<0.01, §§§P<0.001 vs. *Cre*^{Trp1}; ##P<0.01 vs. *Cre*^{Trp1}*;Hif1a*$^{f/f}$; *xx*P<0.01 vs. *Cre*^{Trp1}*;Hif2a*$^{f/f}$. Scale bars: 250µm (A); 500µm (B); 25µm (C, D, F).
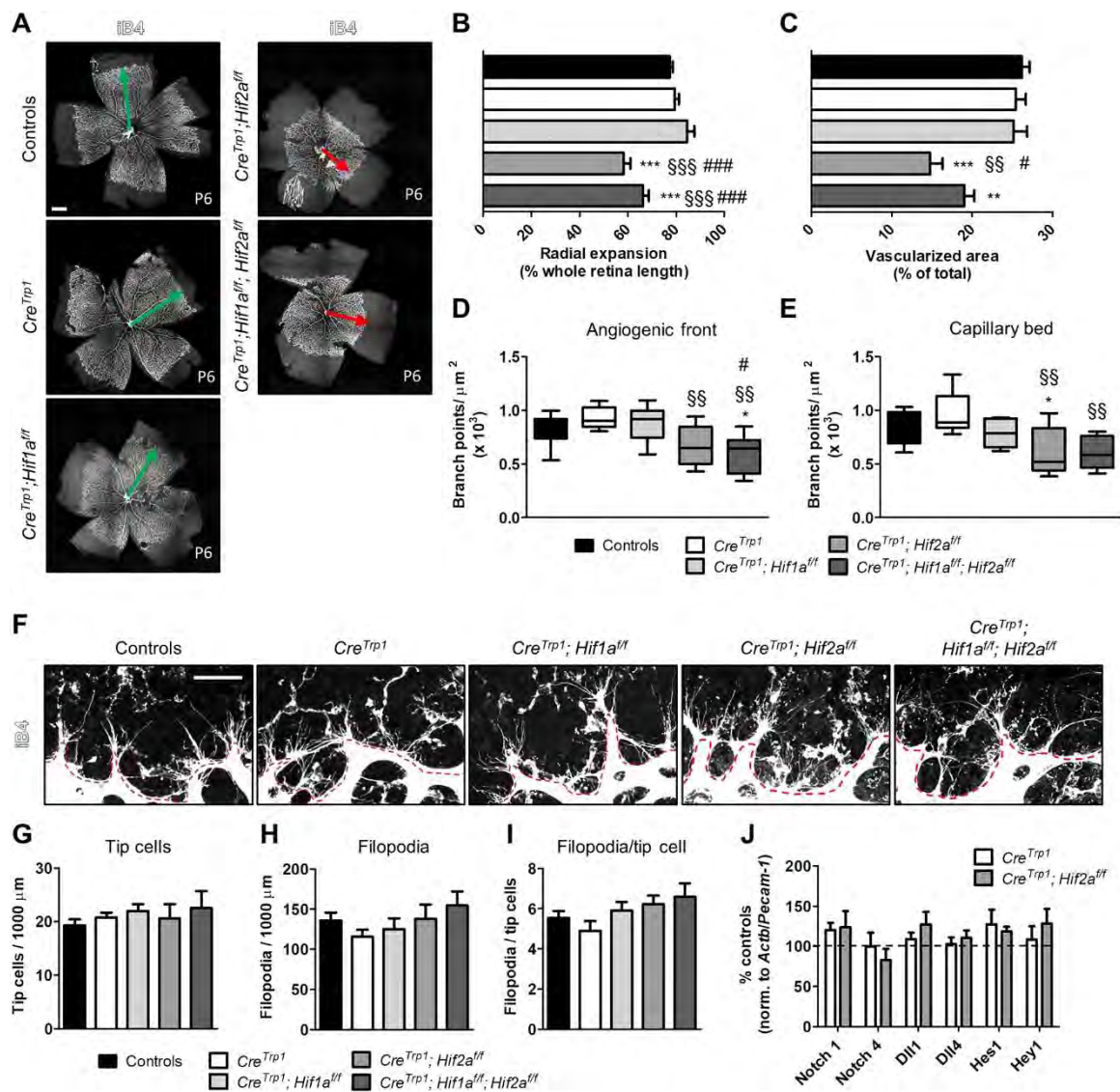
Fig. 3: Deletion of *Hif2a* causes delayed developmental angiogenesis. (A) iB4 staining of whole retinal flatmounts (age: P6) shows a delayed vascular development in *Hif2a* KO lines in terms of radial expansion (B), vascularised area (C), number of branch points in the angiogenic front (D) and in the mature capillary bed (E). n=5-39. Also refer to Fig. S2A. In (D) and (E), whiskers are min and max value; line inside the box is the median. ANOVA and Tukey's multiple comparison test: *$P<0.05$, ***$P<0.001$ vs. controls; §§$P<0.01$, §§§$P<0.001$ vs. *Cre^{Trp1}*; #$P<0.05$, ###$P<0.001$ vs. *Cre^{Trp1};Hif1a$^{f/f}$*. Tip cells and filopodia (F-I) at the angiogenic front (highlighted - red dashed line) for all the genotypes analysed. n=6-19 (4 fields of view/eye). No significant differences (ANOVA). (J) Notch pathway gene expression assessed by RT-qPCR in FACS-sorted (iB4-FITC labelling) endothelial cells (age: P2). Results

expressed as percentage of controls (normalised to endothelial marker *Pecam-1* and housekeeping gene *Actb*); no significant differences (ANOVA). Each sample was a pool of 4-8 retinae; n=3-9. Scale bars: 500μm (A), 25μm (F).
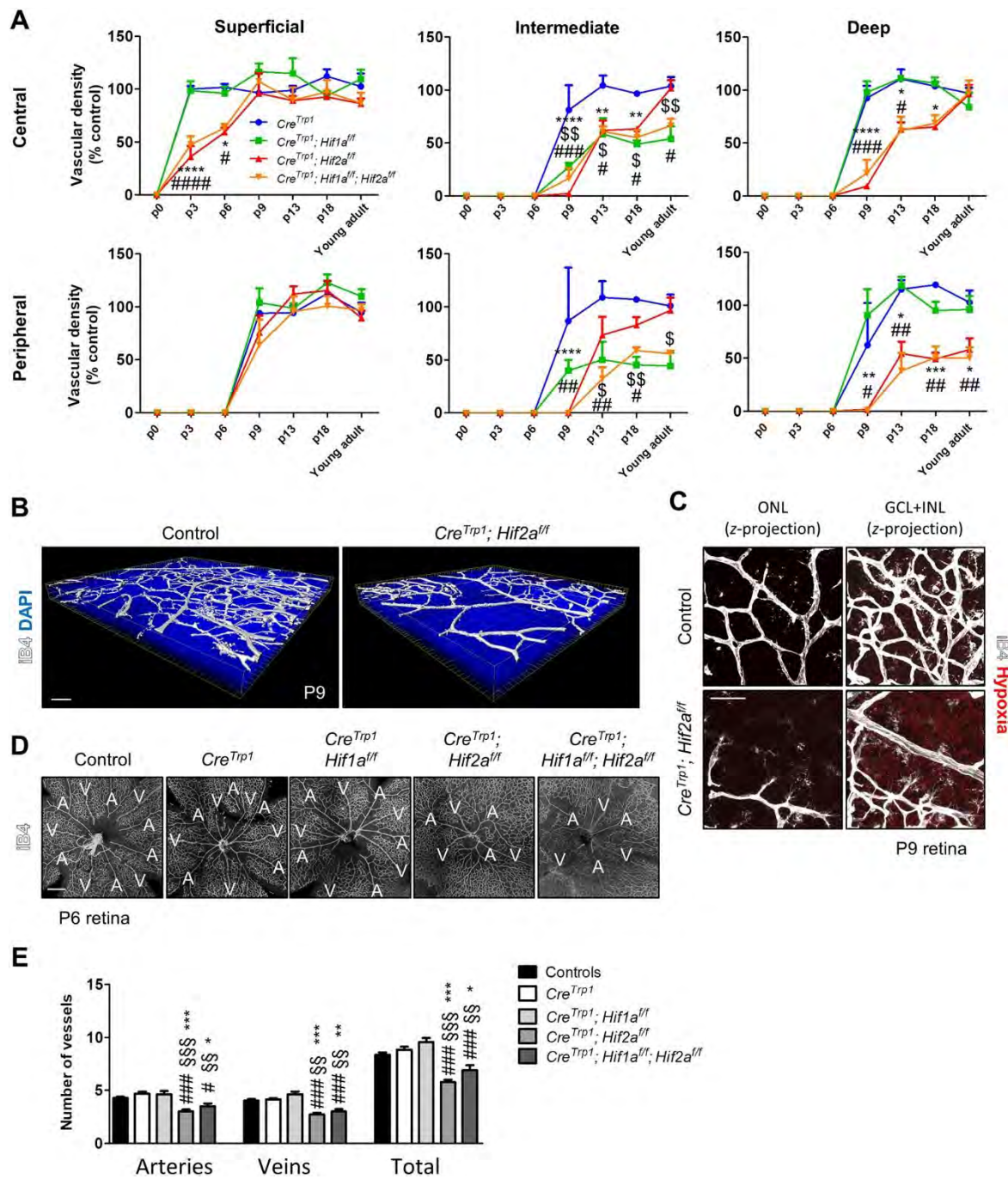
Fig. 4: Vascular phenotype in *Hif2a* KO lines results in delayed plexi formation and fewer arteries and veins. (A) Time-course quantification of deep, intermediate and superficial plexi formation (% of controls). Refer to Fig. S3 for control plexi. n=5-12 animals/genotype/time point. ANOVA and Bonferroni multiple comparison test performed vs. *Cre^Trp1^*: $P<0.05, $$P<0.01 *Cre^Trp1^;Hif1a^f/f^* vs. *Cre^Trp1^*; *P<0.05, **P<0.01, ***P<0.001, ****P<0.0001 *Cre^Trp1^;Hif2a^f/f^* vs. *Cre^Trp1^*; #P<0.05, ##P<0.01, ###P<0.001, ####P<0.0001 *Cre^Trp1^;Hif1a^f/f^;Hif2a^f/f^* vs. *Cre^Trp1^*. (B) *3D* reconstruction

of P9 *Cre^{Trp1};Hif2a^{f/f}* vasculature. (C) Persistent hypoxia between the primary and the deep plexi (GCL and INL). (D) IB4 staining revealing reduction in arteries and veins in *Hif2a* KO lines. Quantification shown in (E). n=8-12. ANOVA and Tukey's multiple comparison test: *$P<0.05$, **$P<0.01$, ***$P<0.001$ vs. controls; §§$P<0.01$, §§§$P<0.001$ vs. *Cre^{Trp1}*; #$P<0.05$, ###$P<0.001$ vs. *Cre^{Trp1};Hif1a^{f/f}*. Scale bars: 50µm (B, C), 200µm (D).
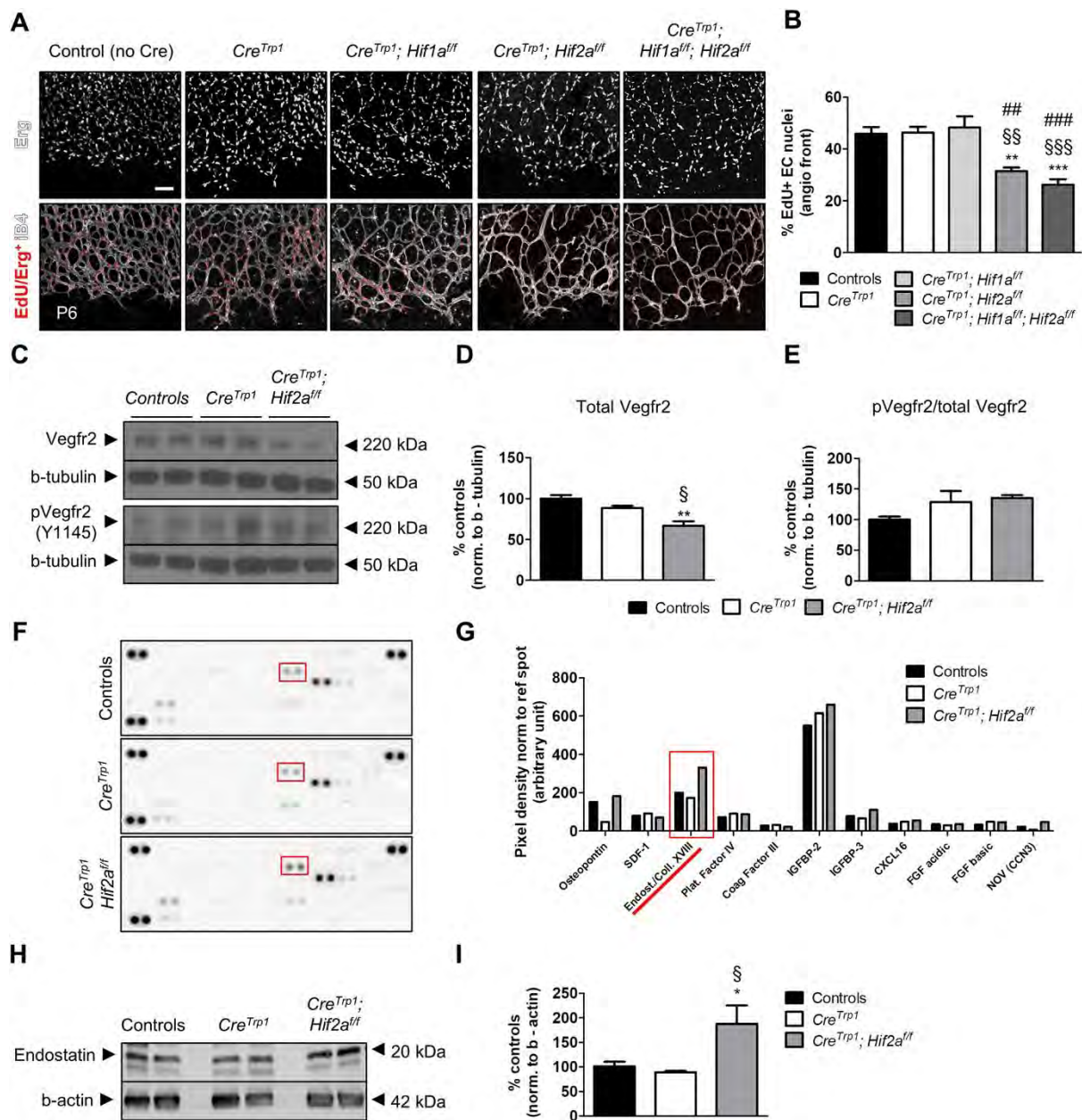
Fig. 5: *Hif2a* KO lines show reduced endothelial cells division, a normal Vegfr2 activation and increased endostatin levels. (A) EdU inclusion in endothelial cells nuclei (stained with Erg) at the angiogenic front (age: P6). Values are quantified in (B). n=5; 4 fields/animal quantified. ANOVA and Tukey's multiple comparison test: **$P<0.01$, ***$P<0.001$ vs. controls; §§$P<0.01$, §§§$P<0.001$ vs. *Cre^{Trp1}*; ##$P<0.01$, ###$P<0.001$ vs. *Cre^{Trp1};Hif1a$^{f/f}$*. (C) Representative western blot of whole retina lysates (age: P5) probed for total Vegfr2, phosphorylated Vegfr2 (Y1145) and b-tubulin. Densitometry reported in (D) and (E). Values expressed as percentage relative to controls; n=4-6. ANOVA and Tukey's multiple comparison test: **$P<0.01$

vs. controls; §$P<0.05$ vs. Cre^{Trp1}. (F) Angiogenesis proteome profiler array of P6 whole retina lysates (pooled n=10 retinae). Densitometry reported in (G). (H) Representative western blot of whole retina lysates (age: P6) probed for endostatin and b-actin. Densitometry reported in (I). Values expressed as percentage relative to controls; n=4-6 animals. ANOVA and Tukey's multiple comparison test: *$P<0.05$ vs. controls; §$P<0.05$ vs. Cre^{Trp1}. Scale bar: 10μm (A).
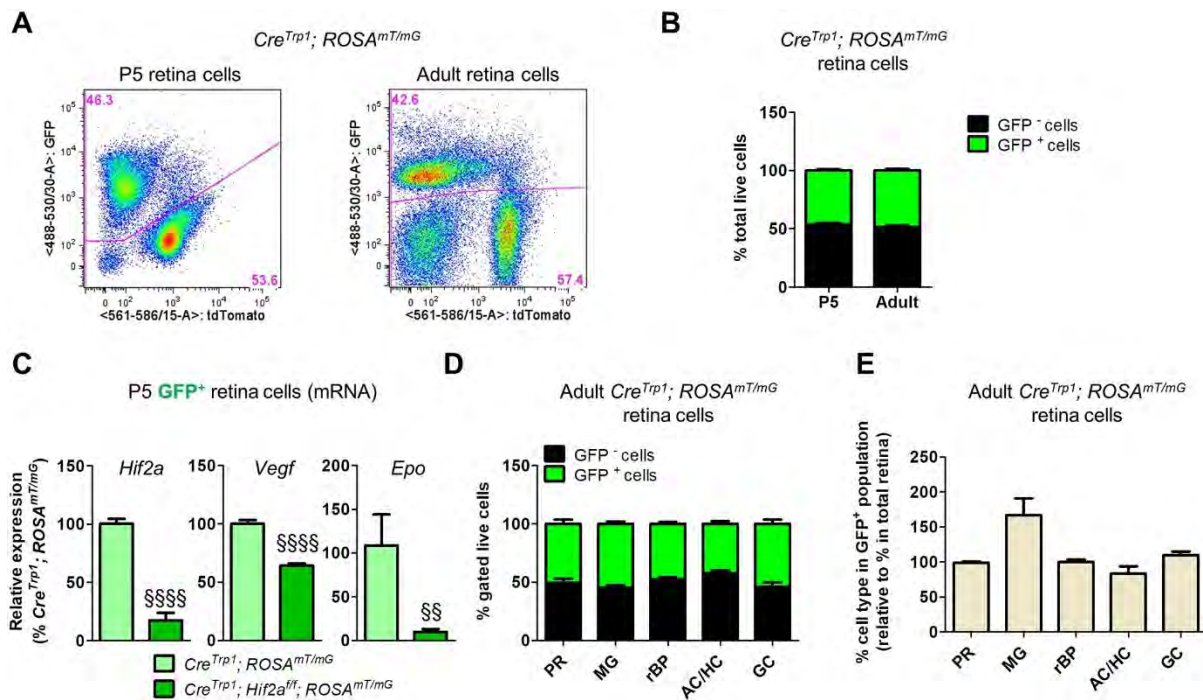
Fig. 6: Characterisation of neuroretina cells expressing *Cre* recombinase in *Cre^Trp1* line. (A) Representative flow cytometry (P5 and young adult) of *Cre^Trp1;ROSA^mT/mG*. (B) Quantification of total live GFP$^+$ and GFP$^-$ cells. n=24-52 animals/age. (C) RT-qPCR analysis of GFP$^+$ cells FACS-sorted from P5 *Cre^Trp1;ROSA^mT/mG*. Targets analysed: *Hif2a*, *Vegf* and *Epo*. n=6-7. ANOVA and Tukey's multiple comparison test: §§P<0.01, §§§§P<0.0001 vs. *Cre^Trp1;ROSA^mT/mG*. (D) Quantification of GFP$^+$ and GFP$^-$ cells for each sub-population analysed by flow cytometry on adult dissociated *Cre^Trp1;ROSA^mT/mG* retinae. Please refer to Table S1-S2 for markers and reference percentages. (E) The histogram compares the composition of the GFP$^+$ sub-population to the composition of the whole retina of adult *Cre^Trp1;ROSA^mT/mG* mice (values expressed as percentage of the total retina composition). n=5-9. PR: photoreceptors; MG: Müller glia; rBP: rod bipolar cells; AC: amacrine cells; HC: horizontal cells; GC: ganglion cells.
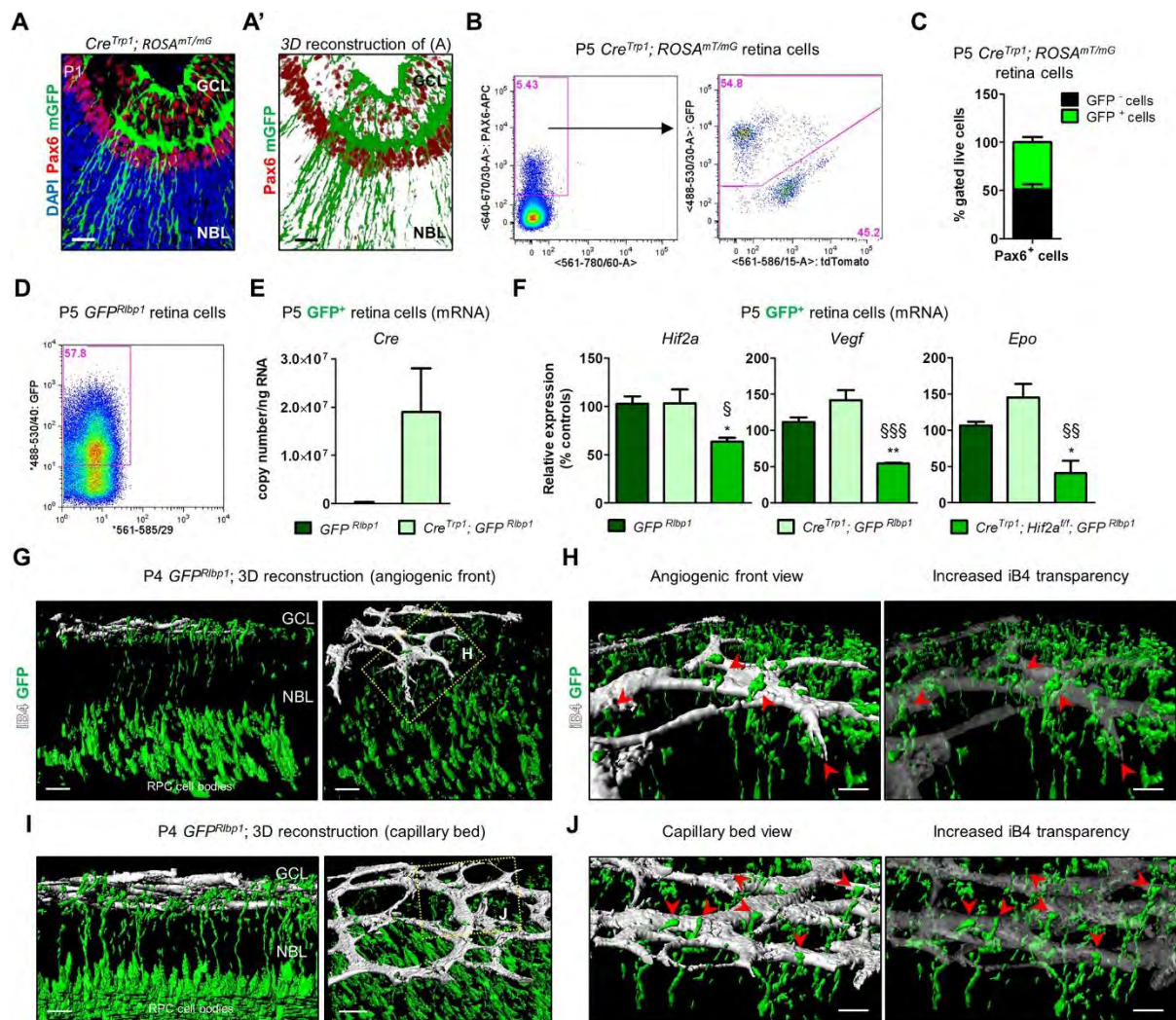
Fig. 7: Cre expression affects late neuroprogenitors in the Cre^{Trp1} line. (A) P1 section from Cre^{Trp1} line showing co-localisation of mGFP$^+$ cells and ganglion cell/neuroprogenitor marker Pax6 (false-coloured in red for better visualisation). mTomato signal not shown. (A') *3D* reconstruction of (A). (B) Representative flow cytometry of P5 Pax6$^+$/mGFP$^+$ cells in P5 $Cre^{Trp1};ROSA^{mT/mG}$ retina. (C) Quantification of GFP$^+$ and GFP$^-$ Pax6$^+$ cells. n=7 animals/age. (D) Representative flow cytometry of GFP$^+$ cells in P5 $Cre^{Trp1};GFP^{Rlbp1}$ retina. (E) RT-qPCR analysis of *Cre* copy number in GFP$^+$ cells FACS-sorted from indicated genotypes (age: P5). Values are from n=5-14. (F) RT-qPCR analysis of *Hif2a* and downstream targets *Vegf* and *Epo* on FACS-sorted GFP$^+$ cells (age: P5). Values are from n=4-5 samples and are normalized to GFP$^+$ cells isolated from GFP^{Rlbp1}. ANOVA and Tukey's multiple comparison test: *$P<0.05$, **$P<0.01$ vs. controls; §$P<0.05$, §§$P<0.01$, §§§$P<0.001$ vs. Cre^{Trp1}. (G) *3D* reconstruction of P4 GFP^{Rlbp1} (two orientations of

same confocal *z*-stack) shows points of contact between GFP$^+$ retinal neuroprogenitors' projections and endothelial cells. Increased transparency helps appreciating the interactions (see red arrows). Similarly, late neuroprogenitors interact with mature capillary bed as shown in (I-J). Scale bar: 25µm (A, A'); 20µm (G, I); 10µm (H, J).
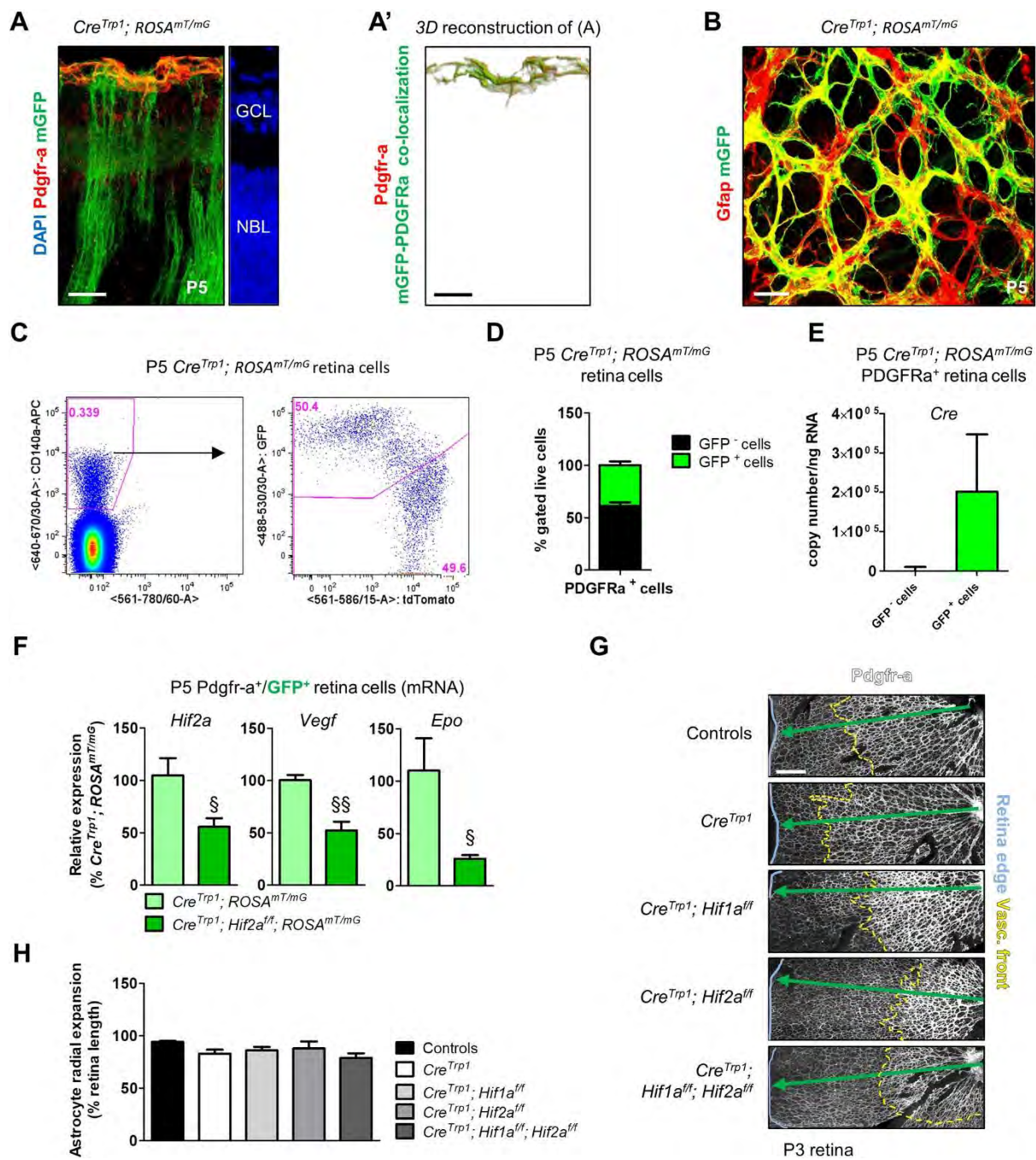
Fig. 8: Although affected by Cre mediated-excision, astrocytes invade the developing retina in a timely manner. (A) P5 section from *Cre^Trp1^;ROSA^mT/mG^* line showing co-localisation between GFP⁺ cells and astrocyte marker Pdgfr-a (false-coloured in red for better visualisation). mTomato signal not shown. (A') *3D* reconstruction of (A). (B) *Z*-stack projection of a P5 flat-mounted retina from *Cre^Trp1^;ROSA^mT/mG^* mouse showing astrocyte marker Gfap (false coloured in red for better visualisation; tdTomato not shown) and mGFP co-localisation. (C)

Representative flow cytometry of Pdgfr-a$^+$/GFP$^+$ cells in P5 *Cre^{Trp1};ROSA$^{mT/mG}$* dissociated retina. (D) Quantification of GFP$^+$ and GFP$^-$ in Pdgfr-a$^+$ cell population. n=13 animals. (E) RT-qPCR analysis of *Cre* copy number in GFP$^+$ and GFP$^-$ FACS-sorted Pdgfr-a$^+$ cells from P5 *Cre^{Trp1};ROSA$^{mT/mG}$*. Values expressed as copy number/ng of retro-transcribed RNA (n=8). (F) RT-qPCR analysis of *Hif2a* and its targets *Vegf* and *Epo* on Pdgfr-a$^+$/GFP$^+$ cells FACS-sorted from P5 *Cre^{Trp1};ROSA$^{mT/mG}$* and *Cre^{Trp1};Hif2a$^{f/f}$;ROSA$^{mT/mG}$* lines. Values are relative percentage of *Cre^{Trp1};ROSA$^{mT/mG}$* (n=4-5). ANOVA and Tukey's multiple comparison test: §$P<0.05$, §§$P<0.01$ vs. *Cre^{Trp1};ROSA$^{mT/mG}$*. (G) Retinal whole-mounts (age: P3) stained with Pdgfr-a. Tissue edges are highlighted with a light blue line, angiogenic front with a yellow dashed line. (H) Quantification of astrocyte radial expansion. n=4-6; 4 fields of view analysed/sample. No significant differences (ANOVA). Scale bars: 25µm (A-B); 200µm (G).
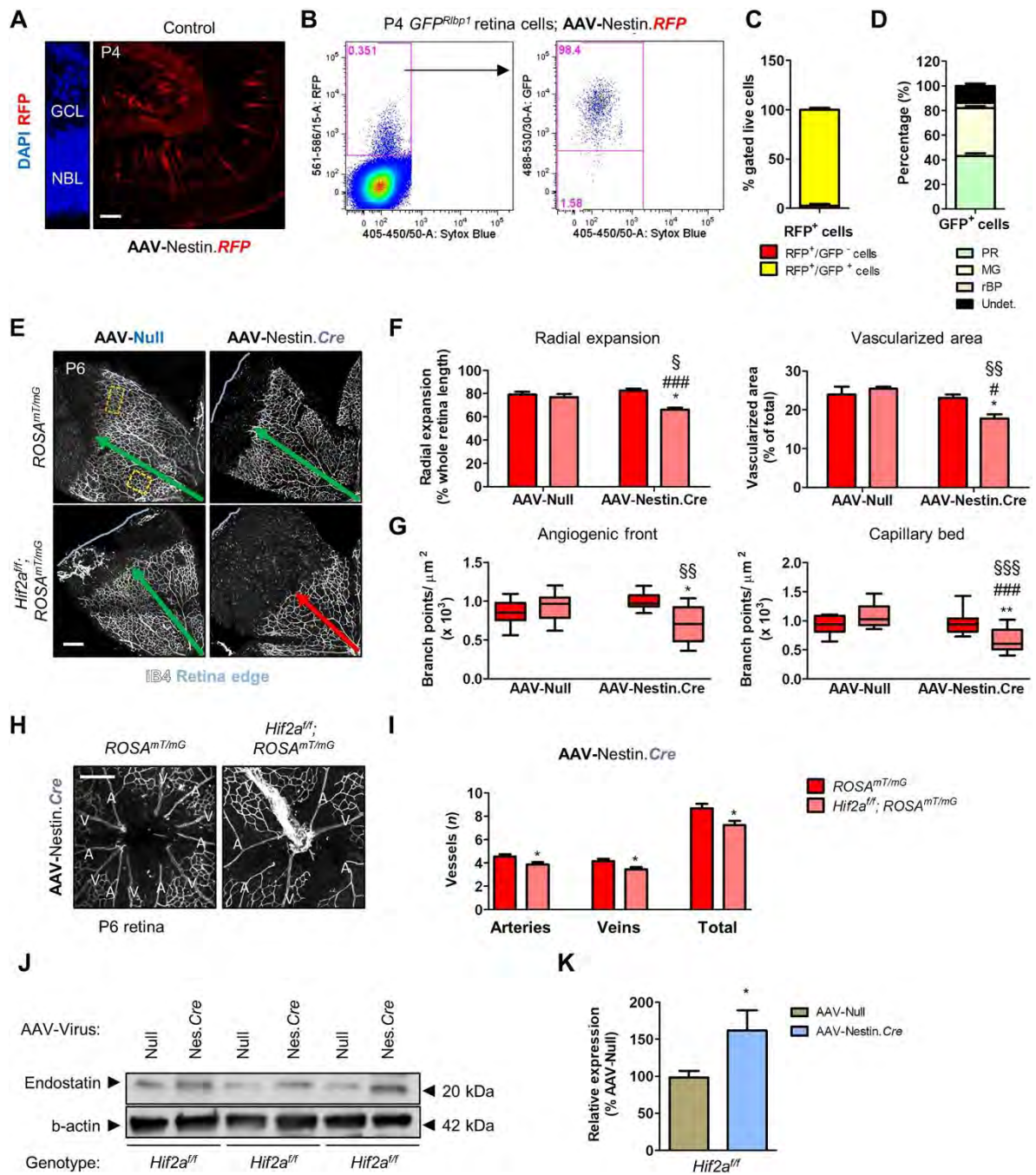
Fig. 9: Viral delivery of Cre recombinase to late neuroprogenitors in the *Hif2a^f/f* **mice recapitulates the vascular phenotype observed in *Cre^Trp1^; Hif2a^f/f*** **mice.** (A) Representative image of a wild-type eye injected with AAV-Nestin.*RFP*. (B) Representative flow cytometry of RFP virus in *GFP^Rlbp1^* mice and (C) quantification of RFP/GFP co-labelling. n=6. (D) Quantification of cell types by flow cytometry of AAV-Nestin.*Cre*-injected *ROSA^mT/mG^* retinae, harvested and dissociated at P18. PR: photoreceptors; MG: Müller glia; rBP: rod bipolars; undet: undetermined. (E) iB4-

stained retinal flatmounts injected with AAV-Nestin.*Cre* in one eye and AAV-Null in the contralateral eye (genotypes indicated). (F) Quantification of vascular development. n=7-20. (G) Quantification of branch points in the angiogenic front and in the mature capillary bed. Orange (angiogenic front) and yellow (capillary bed) boxes in (E) represent examples of fields used for quantification. Values are expressed with box plots (n=7-15) as in Fig. 2D,E. ANOVA and Bonferroni multiple comparison test (F,G): *P<0.05, **P<0.01 vs. *Hif2a$^{f/f}$;ROSA$^{mT/mG}$*/AAV-Null; #P<0.05, ###P<0.001 vs. *ROSA$^{mT/mG}$*/AAV-Null; §P<0.05, §§P<0.01, §§§P<0.001 vs. *ROSA$^{mT/mG}$*/AAV-Nestin.*Cre*. (H) Representative images of arteries and veins. (I) Big vessels quantification. n=7-20. Unpaired *t*-test: *P<0.05 vs. *ROSA$^{mT/mG}$*/AAV-Null. (J) Representative western blot of whole retinae (age: P6) for endostatin and b-actin. AAV-Null-treated eye and AAV-Nestin.*Cre*-treated eye loaded side-by-side. Densitometry reported in (K). Values expressed as percentage relative to controls; n=11. ANOVA and Tukey's multiple comparison test: *P<0.05 vs. AAV-Null treated eyes. Scale bars: 25µm (A); 250µm (E, H).
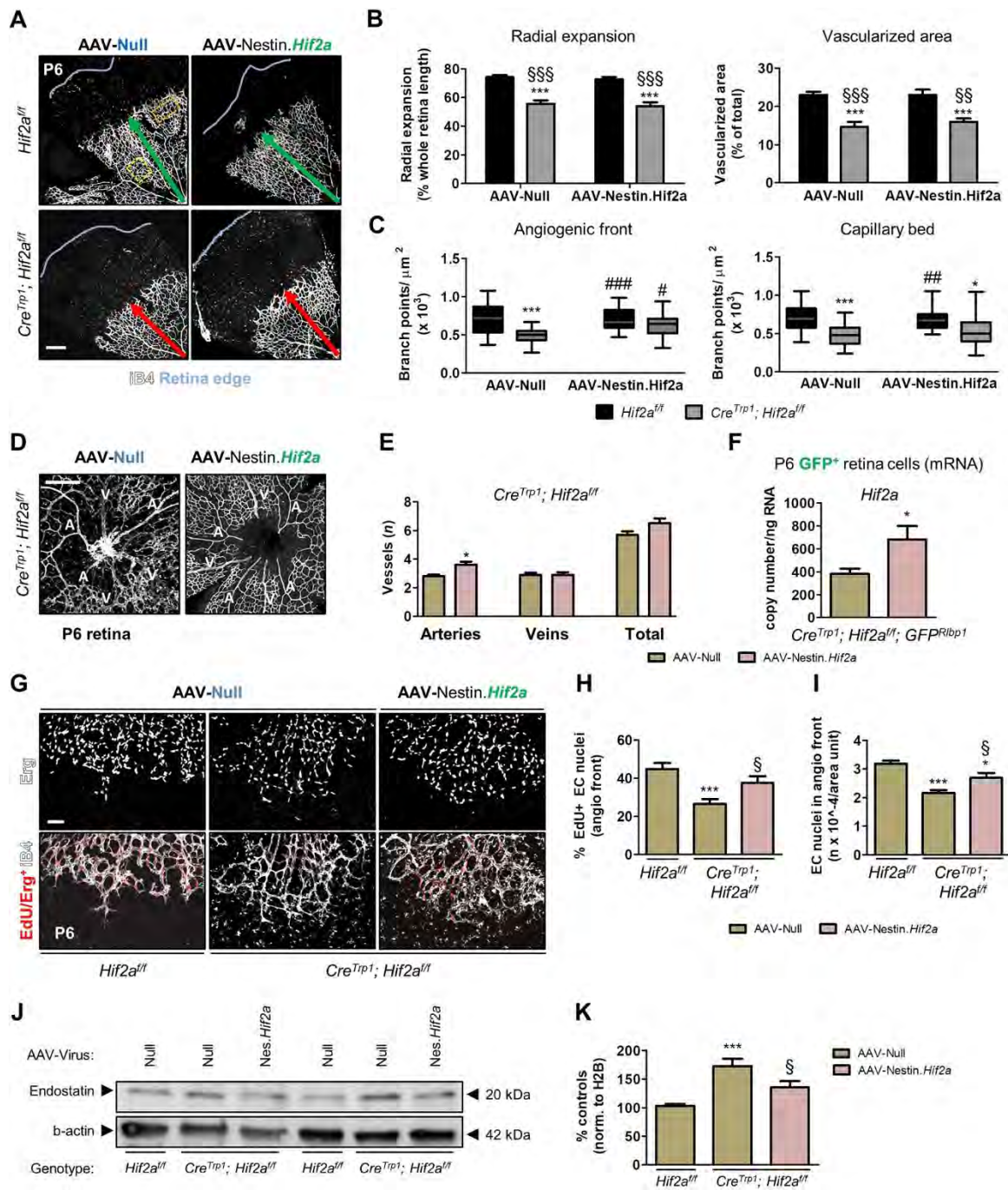
Fig. 10: Delivery of *Hif2a* cDNA to *Cre^Trp1^;Hif2a^f/f^* neuroprogenitors partially rescues the vascular phenotype. (A) Images of iB4-stained retinal flatmounts injected with AAV-Nestin.*Hif2a* and AAV-Null controlaterally (genotypes: *Hif2a^f/f^* and *Cre^Trp1^;Hif2a^f/f^*). (B) Quantification of vascular development in terms of radial expansion and vascularised area. n=10-25. (C) Quantification of branch points in the angiogenic front and in the mature capillary bed. Orange (angiogenic front) and yellow (capillary bed) boxes in (A) represent examples of fields used for

quantification. Values are expressed with box plots (n=14-25) as in Fig. 2D,E. Two-way ANOVA and Bonferroni multiple comparison test (the group upon which the symbol is placed vs. the group indicated in the following description): *P<0.05, ***P<0.001 vs. *Hif2a$^{f/f}$*/AAV-Null; §§P<0.01, §§§P<0.001 vs. *Hif2a$^{f/f}$*/AAV-Nestin.*Hif2a*; ##P<0.01, ###P<0.001 vs. *Cre^{Trp1}; Hif2a$^{f/f}$*/AAV-Null. (D) Arteries and veins in *Cre^{Trp1};Hif2a$^{f/f}$* AAV-injected eyes. (E) Big vessels quantification. n=20-26. Unpaired *t*-test: *P<0.05 vs. AAV-Null. (F) RT-qPCR analysis of *Hif2a* copy number in GFP$^+$ FACS-sorted cells from P6 *Cre^{Trp1};Hif2a$^{f/f}$;GFP^{Rlbp1}* virally injected retinae. Values are expressed as copy number/ng of retro-transcribed RNA (n=6). Unpaired *t*-test: *P<0.05 vs. Null-injected eyes. (G) EdU inclusion in endothelial nuclei (stained with Erg) at the angiogenic front (age: P6). Values are quantified in (H) and in (I); n=9-13; 4 fields/animal quantified. ANOVA and Tukey's multiple comparison test: *P<0.05, ***P<0.001 vs. *Hif2a$^{f/f}$*/AAV-Null; §P<0.05 vs. *Cre^{Trp1};Hif2a$^{f/f}$*/AAV-Null. (J) Representative western blot of whole retina lysates (age: P6) probed for endostatin and b-actin. *Hif2a$^{f/f}$* and *Cre^{Trp1};Hif2a$^{f/f}$* loaded side-by-side are littermates. AAV-Null-treated eye and AAV-Nestin.*Hif2a*-treated eye loaded side-by-side. Densitometry in (K). Values expressed as percentage of controls (n=8). ANOVA and Tukey's multiple comparison test result: ***P<0.001 vs. *Hif2a$^{f/f}$*/AAV-Null eyes; §P<0.05 vs. *Cre^{Trp1};Hif2a$^{f/f}$*/AAV-Null. Scale bar: 250µm (A-D); 100µm (G).
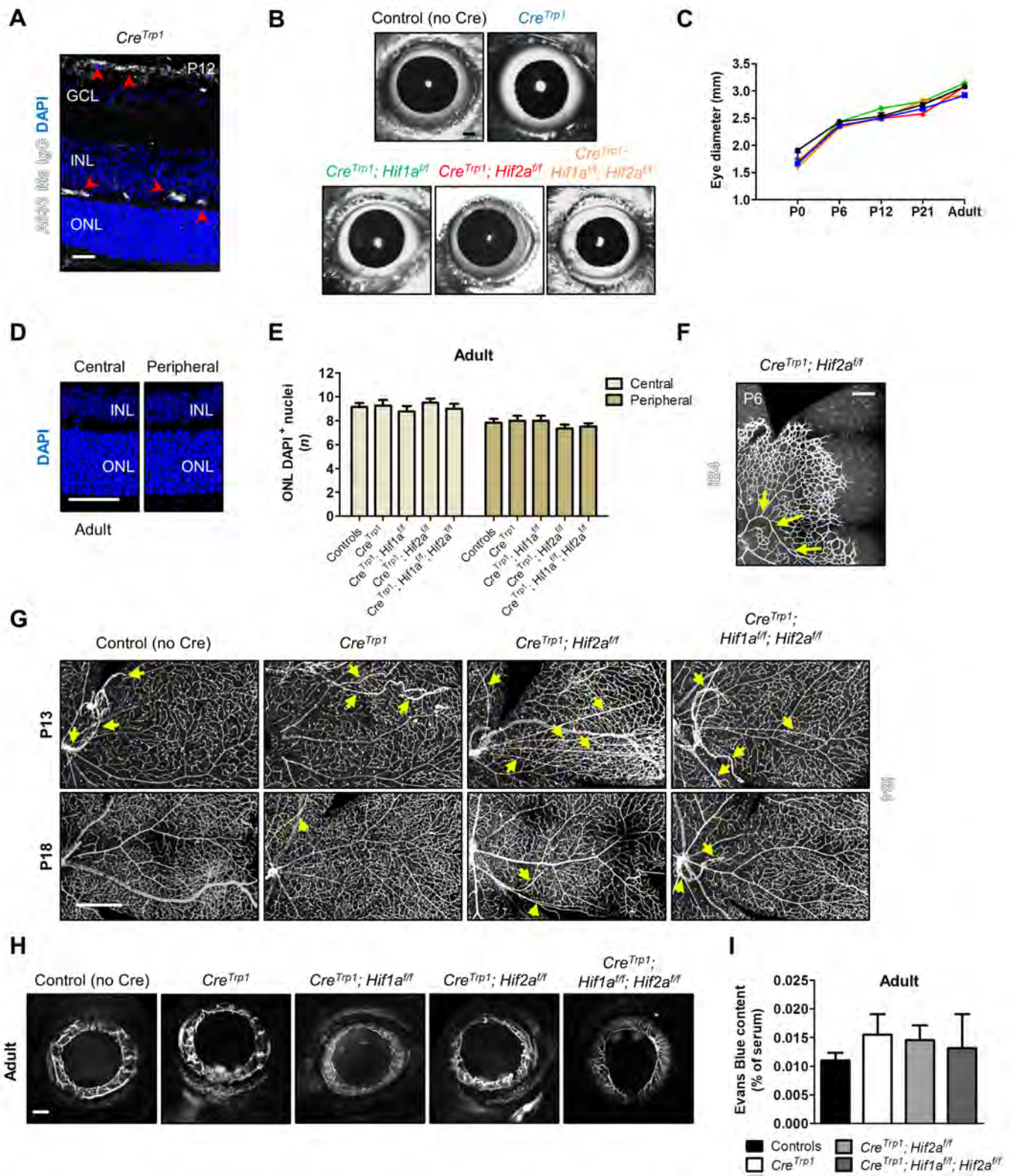
Fig. S1. Deletion of *Hif2a* does not result in eye size changes, photoreceptor degeneration, alterations in iridal vasculature, adult vascular severely persistent hyaloid vasculature or permeability increase. (A) Representative secondary antibody only staining control of P12 *Cre^{Trp1}* eye section. Positive labelling of blood vessels highlighted by red-arrowheads. (B) AF-SLO imaging of representative adult eyes for each genotype analysed. (C) Time-course of post-natal eye growth for the genotypes analysed. Refer to coloured labels in (B). n = 6-12 animals/group. No significant differences observed (ANOVA). (D) Representative images of ONL nuclei in adult eyes and (E) quantification of DAPI$^+$ nuclei rows in the peripheral and central ONL regions (2 pictures/region/animal quantified). n = 4-6 animals/group. No significant differences observed (ANOVA). (F) Representative image of a bended developing artery at P6 of *Cre^{Trp1};Hif2a^{f/f}* genotype (yellow arrows) on a retinal flatmount stained with iB4. (G) iB4 staining of retinal whole mounts, from which the hyaloid vasculature had not been removed, shows some residuals at P13 (yellow arrows) in all genotypes, and very few at P18 in *Hif2a* KO and *Cre^{Trp1}* genotypes. (H) ICGA angiography of the outer portion of the eye shows normal anatomy of the iridal vasculature in all genotypes observed. (I) Evans Blue extravasation assay did not show any significant change in retinal permeability (ANOVA) in *Hif2a* KO genotypes compared to controls and *Cre^{Trp1}*. n = 5-15 animals/group. Scale bars: (A) 25µm (B) 1mm; (D) 50µm; (F) 1mm; (G) 50µm; (H) 25µm.
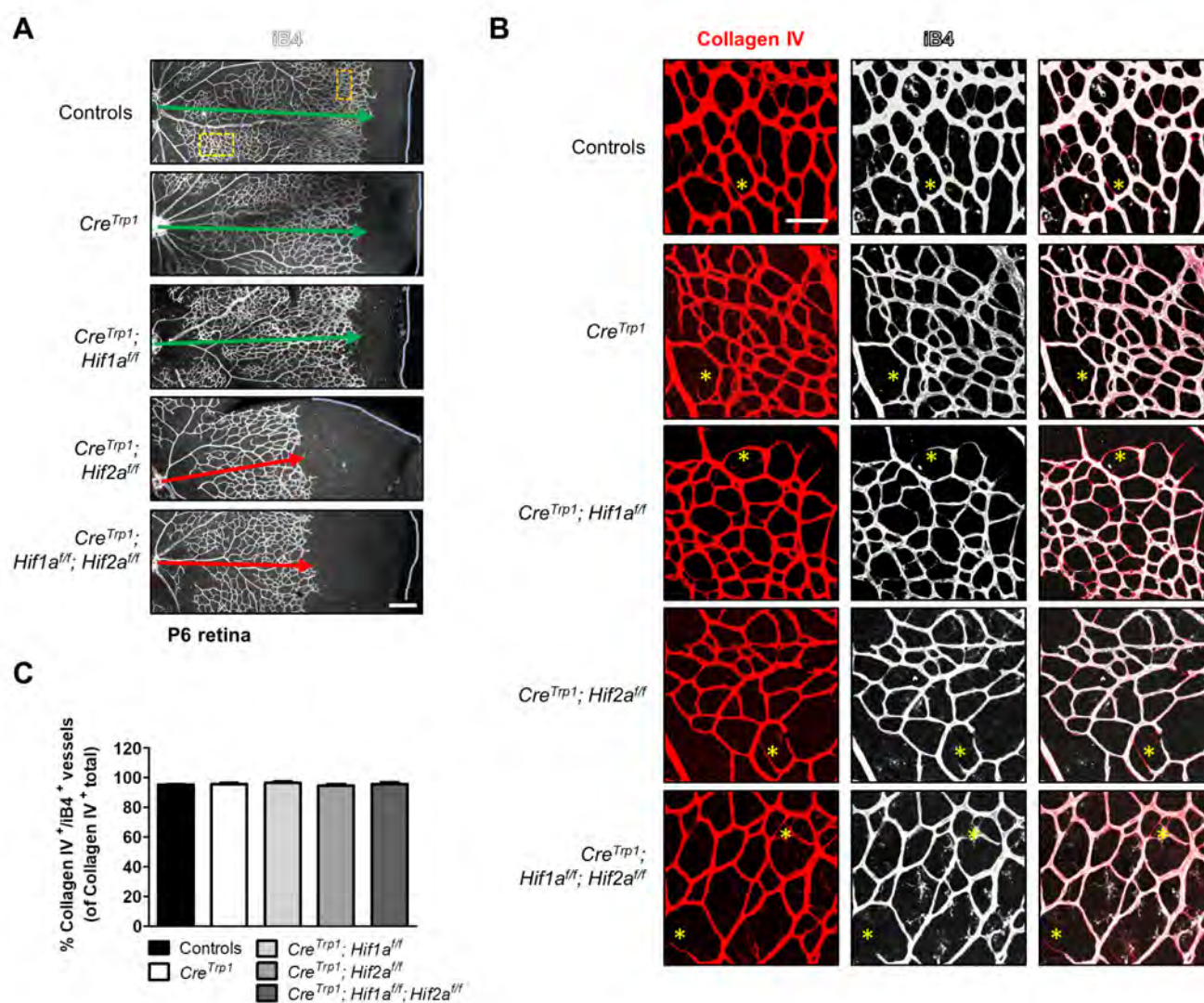
Fig. S2. *Hif2a* deletion does not increase vessel regression. (A) Representative iB4 staining of retinal flatmounts (age: P6) from different genotypes analysed. Orange (angiogenic front) and yellow (capillary bed) boxes in (A) are examples of fields used for branch points quantification in Fig. 3C-D; light blue line indicates the edge of the retina (B) Collagen IV and iB4 staining of P6 retinae. Yellow asterisks show empty Collagen IV sleeves. (C) Quantification of Collagen IV^{+}/iB4^{+} vessels (4 fields/animal measured). Results are from n = 5-6 animals/genotype. No significant differences observed (ANOVA). Scale bars: 250µm (A), 75µm (B).
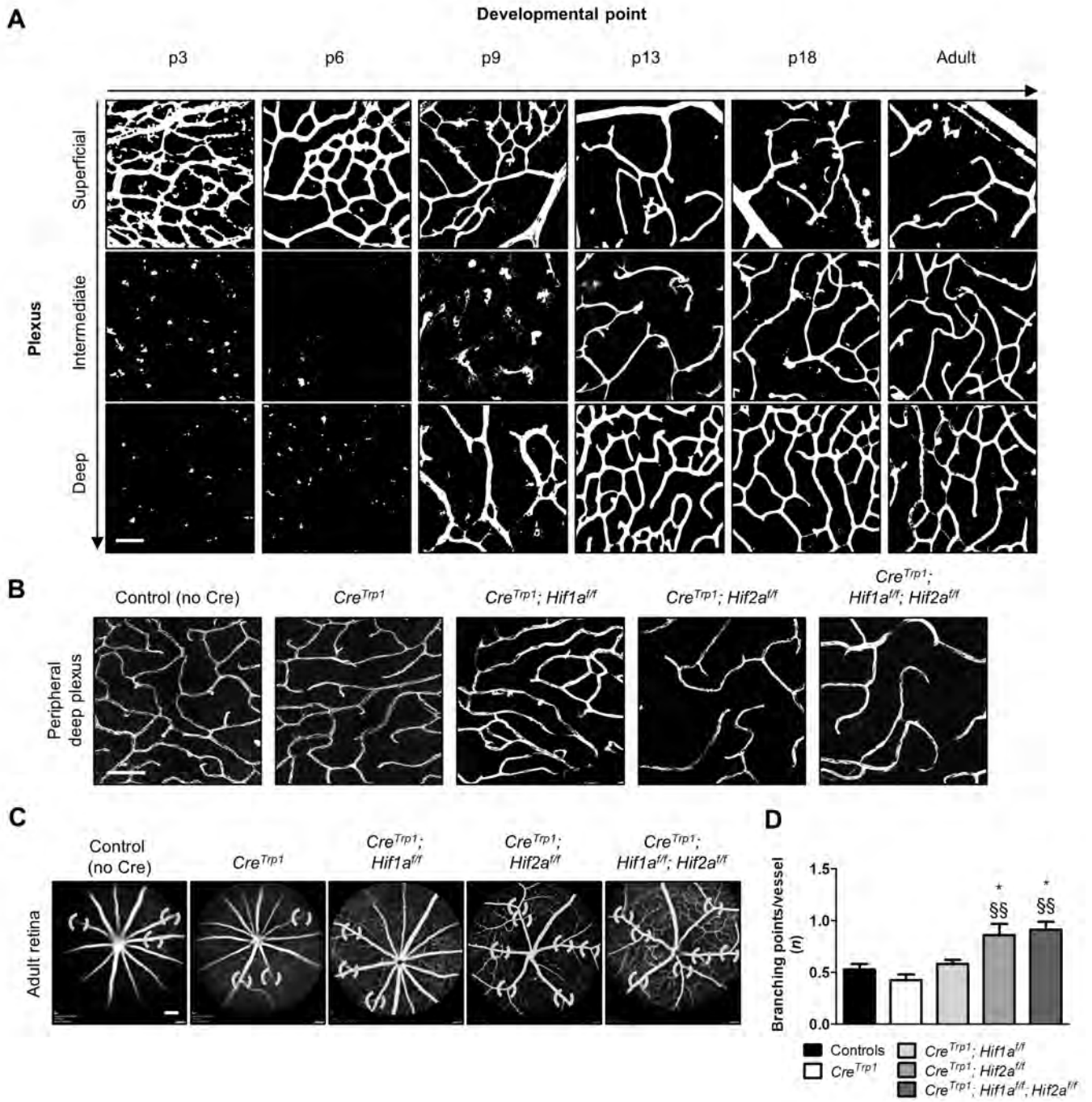
Fig. S3. Wild-type vascular plexi development; peripheral deep plexus abnormalities in adult *Hif2a* KO lines; increased number of major vessels branch points in *Hif2a* KO lines. (A) Representative confocal pictures of iB4 staining of retinal flatmounts, representative of normal central retina plexi development over time (P3 to adulthood). Average density values (n = 5-12 time point) of the controls group were used as reference to calculate vascular development in other genotypes. (B) Representative confocal pictures of adult permanent peripheral deep plexus alterations in *Hif2a* KO lines. (C) Representative AF-SLO pictures of adult animals, showing an increased number of branch points arising from major vessels (light-blue circles). Differences are quantified in (D). n = 7-14 animals/group. ANOVA and Tukey's multiple comparison test results: *$P<0.05$ vs. controls; §§$P<0.05$ vs. Cre^{Trp1}. Scale bars: (A) 75µm; (B) 75µm; (C) 1mm.
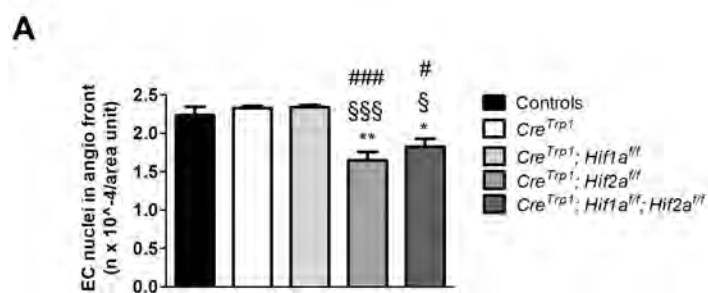
Fig. S4. Decreased number of endothelial cells at the angiogenic front in the developing vasculature of *Hif2a* KO lines. (A) Quantification of endothelial cells nuclei (stained with Erg) at the angiogenic front (representative images in Fig. 4A). n=5 animals/group; 4 fields/animal quantified. ANOVA and Tukey's multiple comparison test results: $*P<0.05$, $**P<0.01$ vs. controls; $\S P<0.05$, $\S\S\S P<0.001$ vs. Cre^{Trp1}; $\#P<0.05$, $\#\#\#P<0.001$ vs. $Cre^{Trp1};Hif1a^{f/f}$.

Fig. S5. Example of flow cytometry analysis of cell markers used to characterise the cellular composition of dissociated whole retina. (A) Flow cytometry gating stra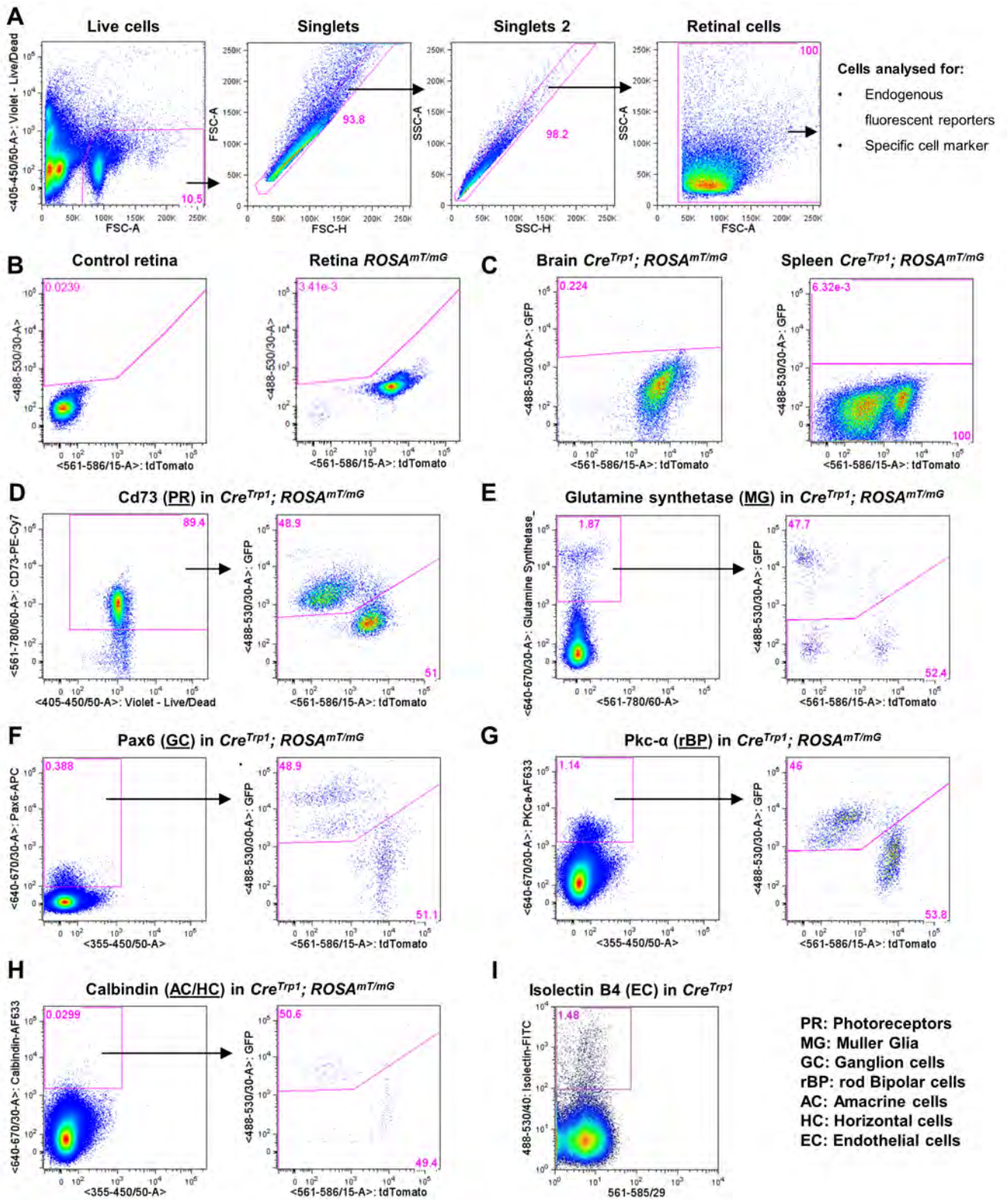tegy for analysis of dissociated retinal samples. This example shows a young adult (4-6 weeks of age) dissociated retina stained with DraQ7 to exclude dead cells and cellular debris and identify the live cell population, which was then plotted to exclude cellular aggregates and to identify only single cells ("singlets" and "singlets 2"). Relative size (FSC-A) and granularity (SSC-A) of single, live retinal cells is then obtained before proceeding to endogenous fluorescent markers and/or antibody staining detection and analysis. (B) Representative plots of control and $ROSA^{mT/mG}$ retinal samples. GFP$^+$ gate is comparable to the one used to analyse $Cre^{Trp1};ROSA^{mT/mG}$ retinae. (C) Representative plots of $Cre^{Trp1};ROSA^{mT/mG}$ brain and spleen samples. (D) Representative plot of CD73 staining on $Cre^{Trp1};ROSA^{mT/mG}$ retina, chosen to label photoreceptors, and subsequent GFP/tdTomato analysis on the gated population. (E) Representative plot of glutamine Synthetase (GS$^+$) staining on $Cre^{Trp1};ROSA^{mT/mG}$ retina, selected to label Müller Glia, and subsequent GFP/tdTomato analysis on the gated population. (F) Representative plot of Pax6 staining on $Cre^{Trp1};ROSA^{mT/mG}$ retina, selected to label ganglion cells, and subsequent GFP/tdTomato analysis on the gated population. (G) Representative plot of Pkc-α staining on $Cre^{Trp1};ROSA^{mT/mG}$ retina, selected to label rod bipolar cells, and subsequent GFP/tdTomato analysis on the gated population. (H) Representative plot of Calbindin staining on $Cre^{Trp1};ROSA^{mT/mG}$ retina, selected to label amacrine and horizontal cells, and subsequent GFP/tdTomato analysis on the gated population. (I) Representative plot showing live FITC-iB4$^+$ cells in a control retinal sample; these cells were sorted into TRIzol plus for further mRNA extraction and transcriptome analysis (Fig. 2J).
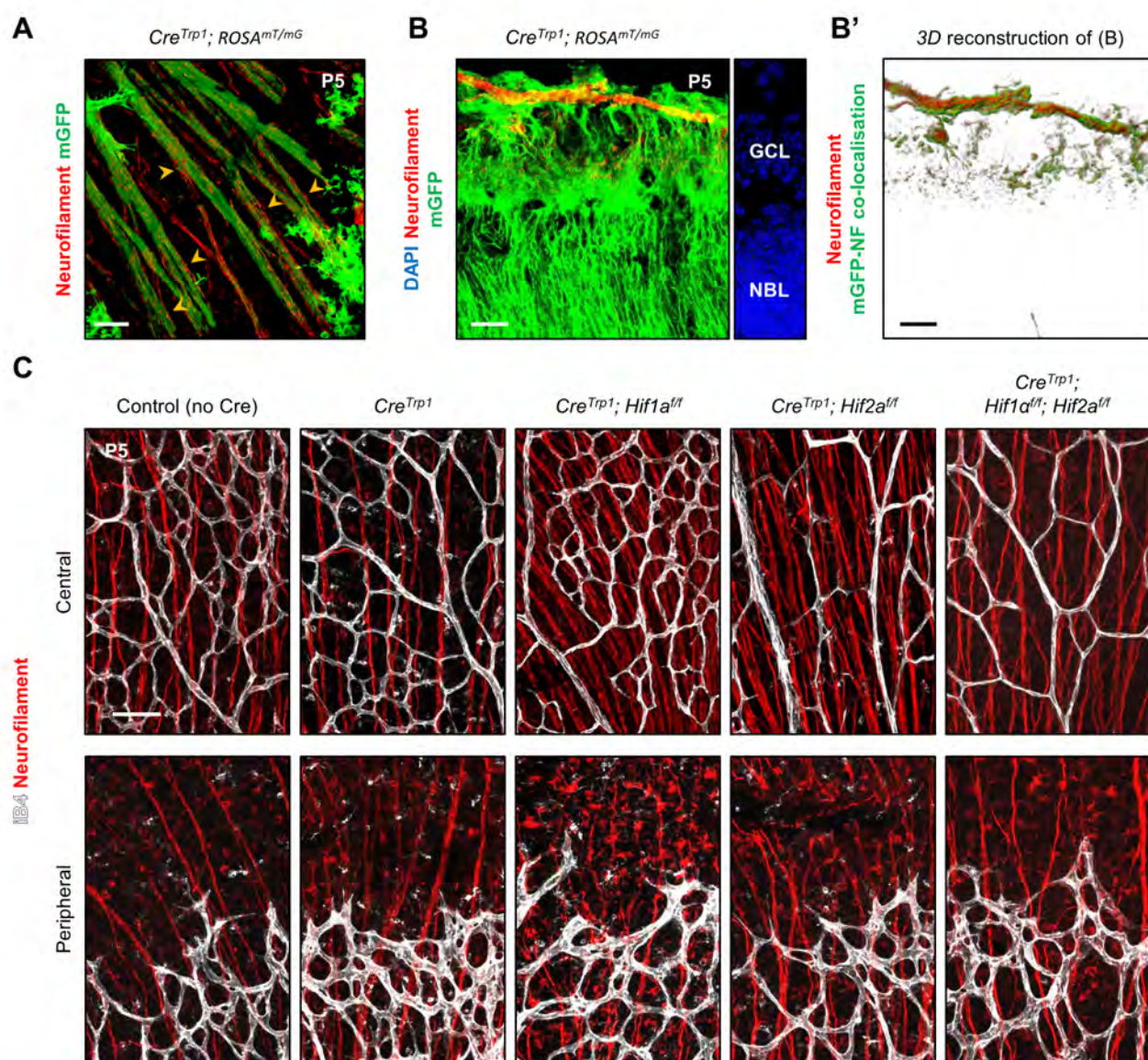
Fig. S6. Ganglion cells axon morphology and spatial organisation are not altered. Confocal images of flatmount (A) and section (B) of P5 *Cre^Trp1^;ROSA^mT/mG^* line showing co-localisation between GFP⁺ cells and retinal ganglion cells marker neurofilament (yellow arrow-heads). (B') Imaris re-construction of (B). (C) Representative confocal images (central retina – mature capillary bed; peripheral – angiogenic front) of immuno-stained ganglion cells and axons, showing normal distribution and morphology in all the genotypes analysed. Scale bars: 25µm (A-B'); 75µm (C).
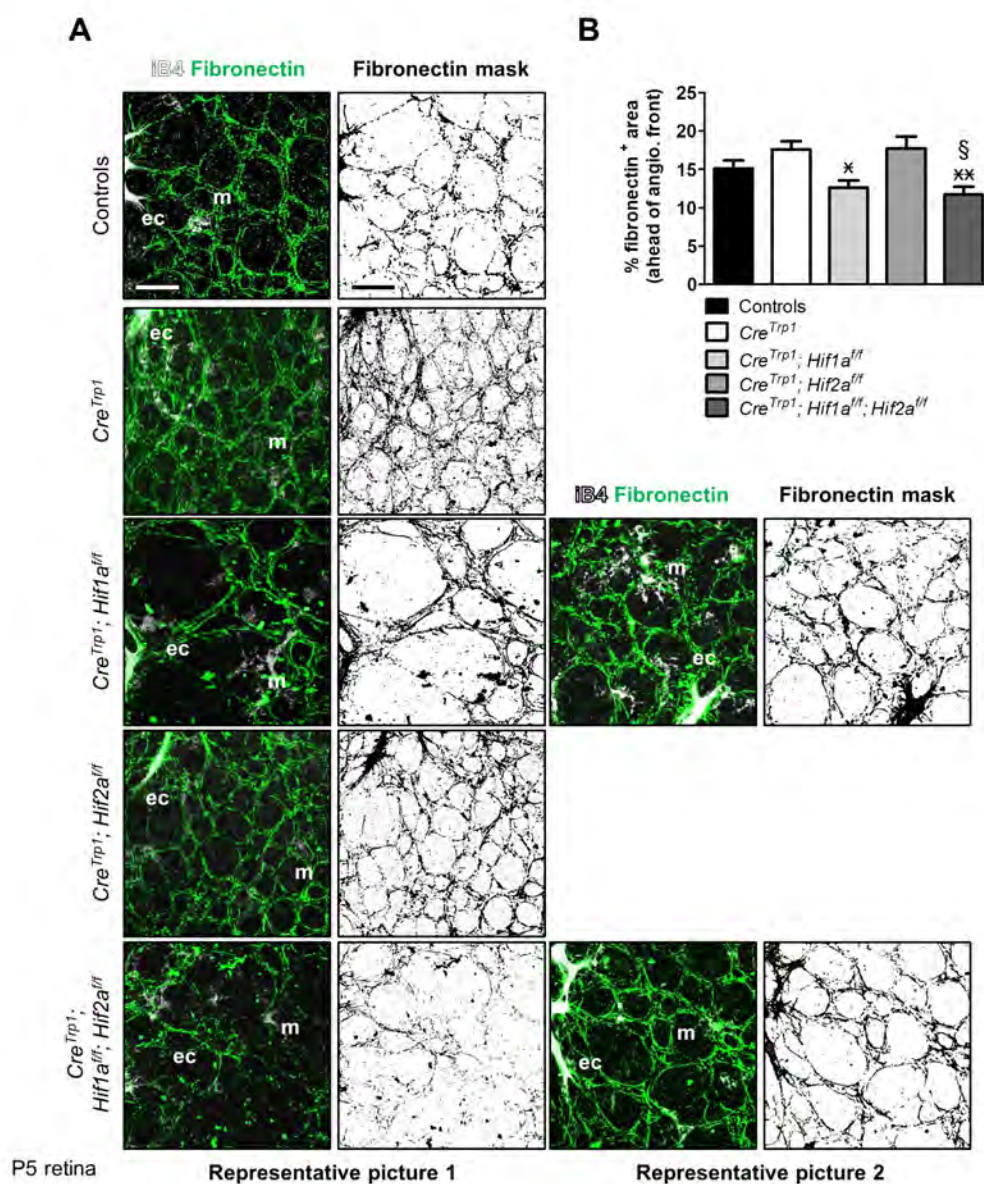
Fig. S7. Astrocyte-mediated fibronectin deposition ahead of the angiogenic front.
(A) Representative images of deposited fibronectin ahead of the angiogenic front (age: P5). Significant differences are only evident in $Cre^{Trp1};Hif1a^{f/f}$ and $Cre^{Trp1};Hif1a^{f/f};Hif2a^{f/f}$, although not in every field of view analysed (see representative picture 2). (B) Quantification of area occupied by fibronectin-positive filaments ahead of the angiogenic front (expressed as percentage of total area analysed). n=5-9 animals/genotype; 4 fields of view/animal. ANOVA and Tukey's multiple comparison test results: §$P<0.05$ vs. Cre^{Trp1}; *$P<0.05$, **$P<0.01$ vs. $Cre^{Trp1};Hif2a^{f/f}$. Scale bar: 25µm (A).

A

P5 *Cre^Trp1; ROSA^mT/mG* retina cells

B

P5 *Cre^Trp1; ROSA^mT/mG*
retina cells

GFP⁻ cells
GFP⁺ cells

C

Control   *Cre^Trp1*   *Cre^Trp1; Hif1a^f/f*   *Cre^Trp1; Hif2a^f/f*   *Cre^Trp1; Hif1a^f/f; Hif2a^f/f*

IB4 Ng2

D

Controls
Cre^Trp1
Cre^Trp1; Hif1a^f/f
Cre^Trp1; Hif2a^f/f
Cre^Trp1; Hif1a^f/f; Hif2a^f/f

E

P5 *Cre^Trp1; ROSA^mT/mG* retina cells

F

P5 *Cre^Trp1; ROSA^mT/mG*
retina cells

GFP⁻ cells
GFP⁺ cells

G

Control (no Cre)   *Cre^Trp1*   *Cre^Trp1; Hif1a^f/f*   *Cre^Trp1; Hif2a^f/f*   *Cre^Trp1; Hif1a^f/f; Hif2a^f/f*

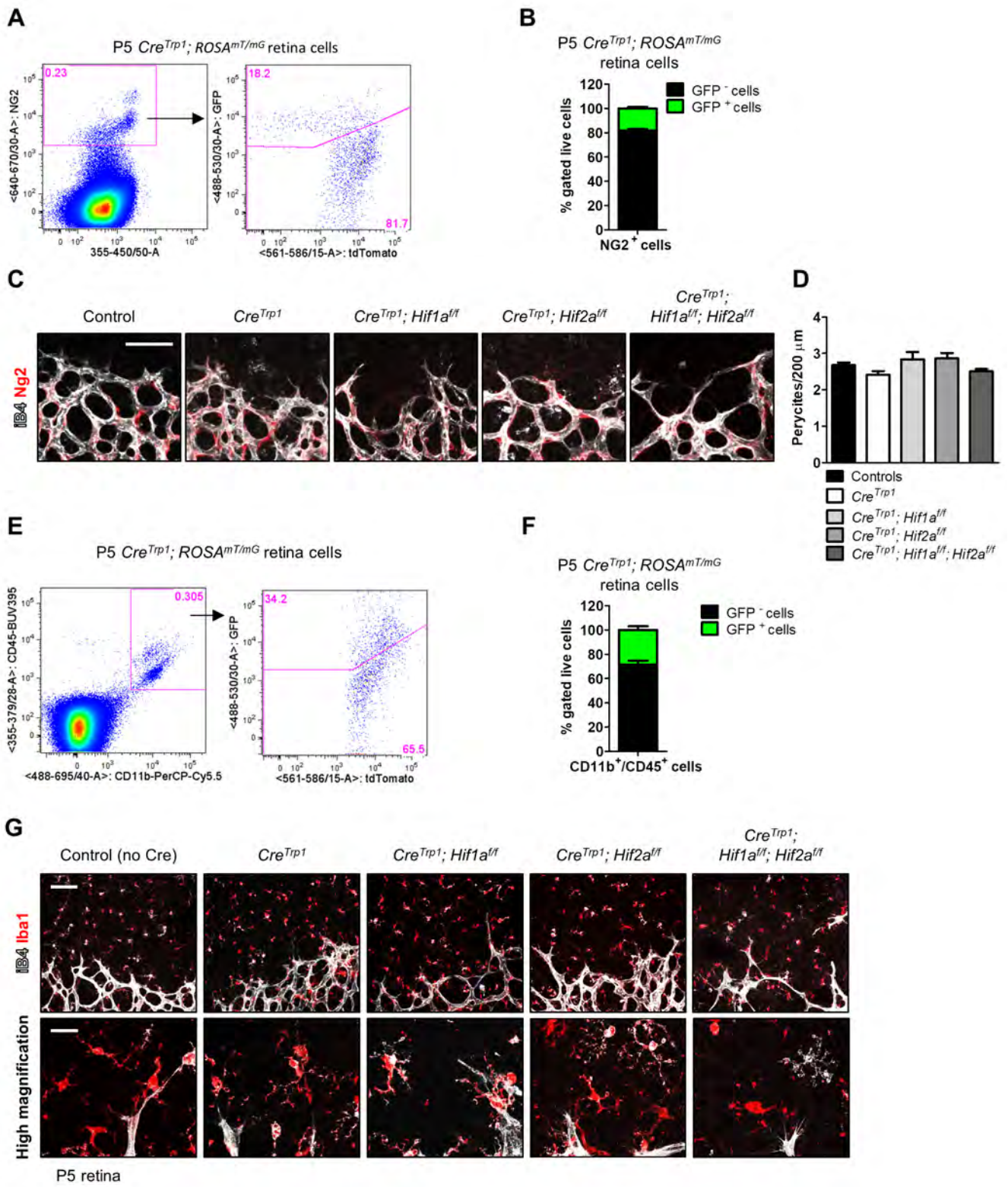IB4 Iba1

High magnification

P5 retina

Fig. S8. Pericytes and resident microglia are partially affected by Cre expression in Cre^{Trp1} lines but their spatial organisation and morphology at the angiogenic front is unaltered. (A) Representative flow cytometric plot of Ng2/GFP$^+$ cells in P5 $Cre^{Trp1};ROSA^{mT/mG}$. (B) Quantification of GFP$^+$ and GFP$^-$ Ng2$^+$ cell population. n=5 animals/genotype. (C) Normal distribution of Ng2$^+$ pericytes at the angiogenic front (age: P5). (D) Quantification of pericytes density. n=5-6 animals/genotype; 4 fields of view/animal. No significant differences between genotypes (ANOVA). (E) Representative flow cytometric plot of CD11b/CD45/GFP$^+$ cells in P5 $Cre^{Trp1};ROSA^{mT/mG}$. (F) Quantification of GFP$^+$ and GFP$^-$ CD11b/CD45$^+$ cell population. n=5 animals. (G) Representative images at the angiogenic front showing normal presence of Iba1$^+$ resident myeloid cells and higher magnification to appreciate cellular morphology. Scale bar: 75µm (C, G); 25µm (G high magnification).
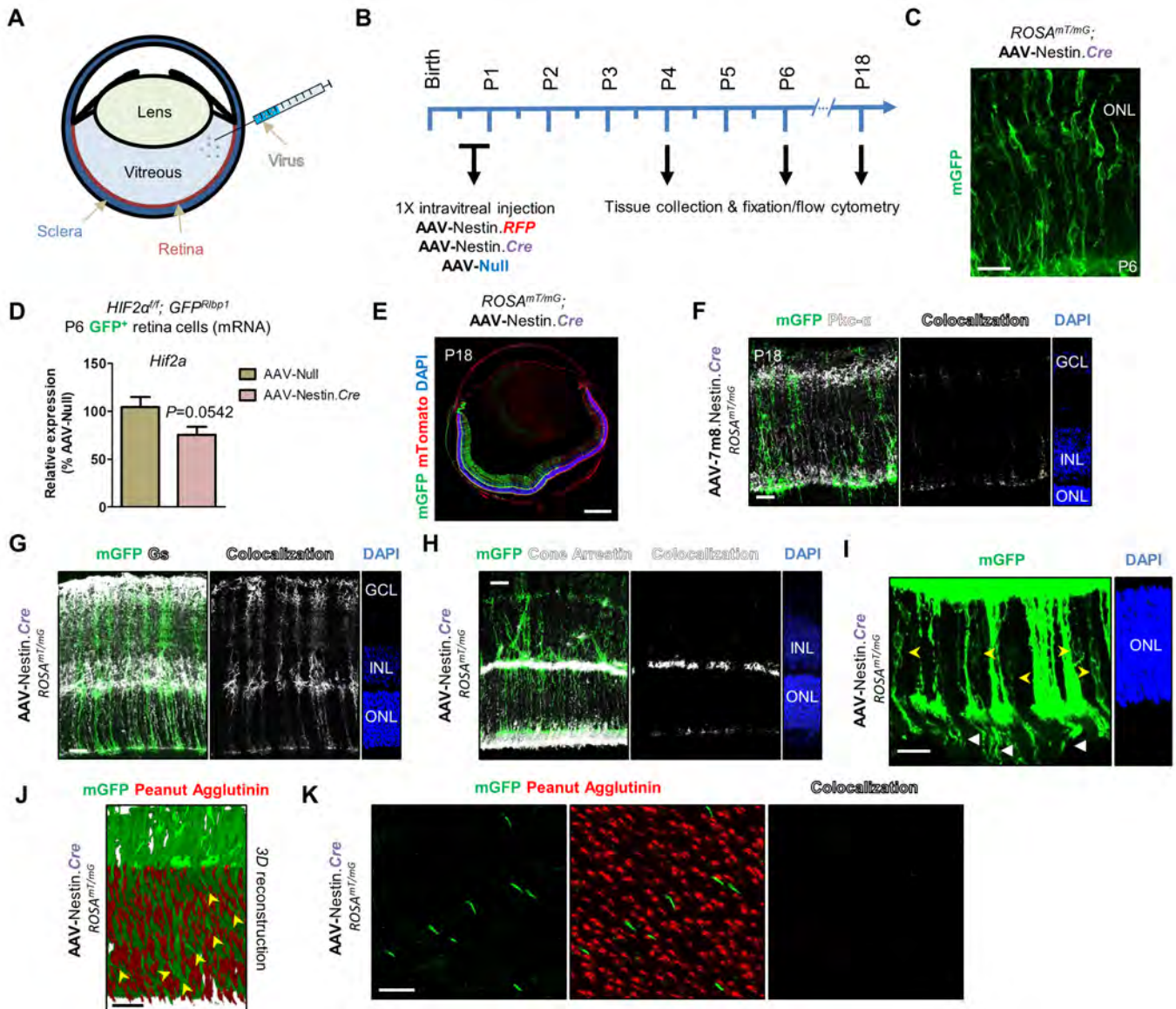
Fig. S9. AAV-Nestin.*Cre* targets late progenitor cells. (A) Schematic describing intravitreal micro-injection. (B) Experimental time-line. For vasculature development experiments, one eye was injected with AAV-Nestin.*Cre*, whereas the controlateral with AAV-Null. (C) Representative image of P6 *ROSA$^{mT/mG}$* injected with AAV-Nestin.*Cre*. (D) RT-qPCR analysis of *Hif2a* in GFP$^+$ cells FACS-sorted from P6 control *Hif2a$^{f/f}$;GFP^{Rlbp1}* eyes injected with either AAV-Null or AAV-Nestin.*Cre*. Values are expressed as percentage relative to Null injected and are from n = 7 animals/group. Unpaired *t*-test result indicated. (E) P18 *ROSA$^{mT/mG}$* eye injected intravitreally with AAV-Nestin.*Cre* virus. Sections were then stained with Pkc-α (F), Glutamine Synthetase (GS) (G) and cone arrestin (H). GFP signal convincingly co-localises with GS$^+$ cells (Müller glia), only minimally with Pkc-α, whereas any co-localisation with cone arrestin is produced by random juxtaposition of the two stains. (I) Rod photoreceptor cell bodies are evident in the ONL of a P18 virally-treated *ROSA$^{mT/mG}$* eye (yellow arrow-heads), as well as the outer segments (white arrow-heads). (J) *3D* reconstruction of a fine *z*-stack acquired from a P18 virally-treated *ROSA$^{mT/mG}$* retina, showing cells derived from virally-targeted cells (GFP$^+$) and cones outer segments (PNA-stained). (K) *Z*-projection of the outer segments layer shows no co-localization between GFP$^+$ segments and cone segments. Scale bars: 25µm (C, F-K); 500µm (E).
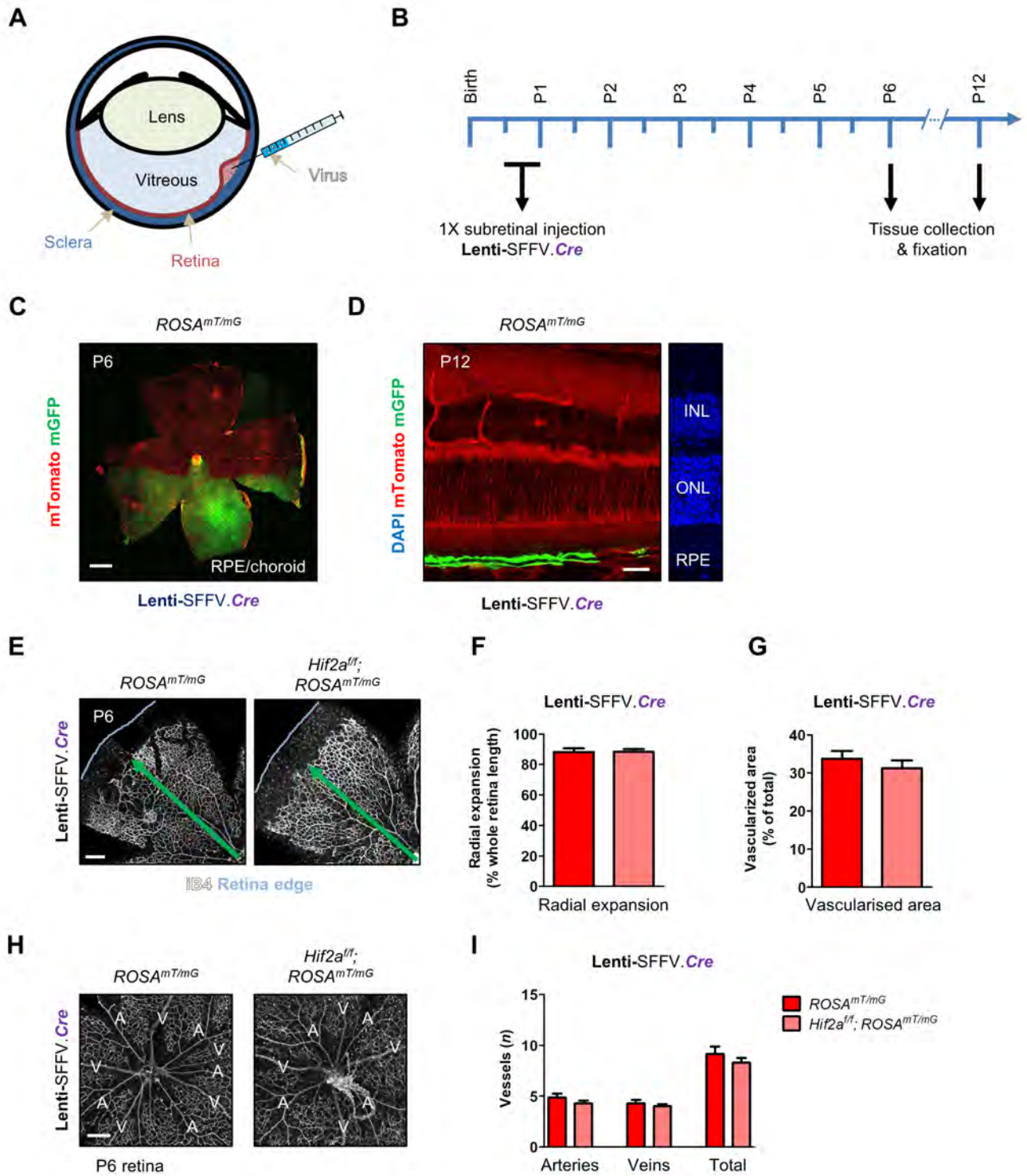
Fig. S10. RPE-targeted delivery of *Cre* recombinase to *Hif2a^f/f* line does not replicate the vascular phenotype observed in *Cre^Trp1;Hif2a^f/f* mice. (A) Schematic describing subretinal micro-injection. (B) Experimental time-line. (C) Representative RPE/choroid flatmount (age: P6; *ROSA^mT/mG* genotype) showing mGFP⁺ areas targeted by lentiviral-mediated Cre recombinase delivery. (D) Section from an eye injected with Lenti.VSVG.SFFV.*Cre* (age: P12; *ROSA^mT/mG*). (E) Representative confocal images of iB4-stained P6 retinal flatmounts injected with Lenti.VSVG.SFFV.*Cre* (genotypes: *ROSA^mT/mG*; *Hif2a^f/f;ROSA^mT/mG*). (F) and (G) show quantification of vascular development (age: P6) in terms of radial expansion and vascularised area. Only retinal regions above strongly transduced RPE regions were quantified. n=8 animals/group. No significant differences between groups (unpaired *t*-test). (H) Arteries and veins in virally-injected eyes (age: P6). (I) Big vessels were quantified and compared (by unpaired *t*-test; no difference). Scale bars: 500µm (C); 25µm (D); 250µm (E, H).

Marker(s)	Cell target	Abbreviation	Reference
CD73	Photoreceptors	PR	Koso et al., 2009
Glutamine Synthetase	Müller glia	MG	Grossman et al., 1994
Pkc-a	Rod bipolar cells	rBP	Ruether et al., 2010
Calbindin	Amacrine/ Horizontal cells	AC/HC	Liu et al., 2013
Pax6	Ganglion cells/retinal progenitor cells	GC/RPC	Hitchcock et al., 1996; Stanescu-Segall et al., 2015
PDGFR-a	Astrocytes	A	Tao and Zhang, 2014
CD11b/CD45	Myeloid cells	MC	Liyanage et al., 2016
NG2	Pericytes	P	Ozerdem et al., 2001

Supplemental Table S1: Markers used by flow cytometry for cell type characterisation.

Markers used for immuno-staining of *Cre* ^{Trp1} ; *ROSA* $^{mT/mG}$ neuroretinae are listed and referenced.

Adult retina	% of total *Cre*^{Trp1} ; *ROSA*$^{mT/mG}$ retina (live events)	% GFP$^+$ population in *Cre*^{Trp1} ; *ROSA*$^{mT/mG}$ retina (live events)	Reference % from (Jeon et al., 1998; Macosko et al., 2015)
Photoreceptors	82.4	81.3	82.1
Müller glia	1.17	1.82	2.80
Rod Bipolar cells	1.54	1.62	* 7.3
Amacrine/horizontals	0.024	0.020	7.00
Ganglion cells	0.45	0.48	0.50
Astrocytes	0.09	0.07	0.10
Myeloid cells	0.28	0.11	0.20
Pericytes	0.20	0.10	ND
Undetermined	13.82	14.49	7.30
Total	100.00	100.00	100.00

Supplemental Table S2: Comparison of cell type percentages to published values.

Values obtained for each retinal cell type (in adult whole Cre^{Trp1}; ROSA$^{mT/mG}$ retina and GFP+ gated population) are compared to reference values reported in the literature (25, 26)

* Value relative to the entire bipolar cells population (as opposed to only rod bipolar cells, identified by PKCa in this study).

Antigene	Antibody species (fluorescent label)	Supplier (catalogue number)	Application	Dilution	Intracellular/extracellular (FC)
Arrestin 3	Rabbit	Novus Biologicals (NBP1-19629)	IF	1:200	
Collagen IV	Rabbit	Bio-Rad (2150-1470)	IF	1:200	
Cre recombinase	Mouse	Millipore (MAB 3120)	IF	1:100	
ERG	Rabbit	Abcam (ab92513)	IF	1:200	
Fibronectin	Rabbit	Millipore (AB 2033)	IF	1:200	
GFAP	Rabbit	Dako (Z0334)	IF	1:200	
Hif2a	Rabbit	Novus Biologicals (NB100)	IF	1:200	
Iba1	Rabbit	Alpha Labs (019-19741)	IF	1:1000	
Isolectin B4 (biotin-conjugated)	N/A	Sigma-Aldrich (L2140)	IF	1:200	
Neurofilament-L	Rabbit	Millipore (C28E10)	IF	1:500	
Beta-Actin	Mouse	R&D Systems (MAB8929)	WB	1:5000	
Beta-Tubulin	Mouse	Sigma-Aldrich (T4026)	WB	1:1000	
Endostatin	Goat	R&D Systems (AF570-SP)	WB	1:1000	
Total VEGFR2	Rabbit	Cell Signalling (9698)	WB	1:1000	
VEGFR2 pY1175	Rabbit	Cell Signalling (3770)	WB	1:1000	
Calbindin	Mouse	Abcam (ab75524)	FC	1:50	Intracellular (fixed)
CD11b	Rat (PerCP-Cy5)	Biolegend (101227)	FC	1:100	Extracellular (unfixed)
CD45	Rat (BUV-395)	BD Biosciences (565967)	FC	1:100	Extracellular (unfixed)
CD73	Rat (PE-Cy7)	Thermo Fisher Scientific (25-0731-80)	FC	1:100	Extracellular (unfixed)
Glutamine synthetase	Mouse	BD Biosciences (610517)	IF/FC	1:200 (IF)/1:50 (FC)	Intracellular (fixed)
Isolectin B4 (FITC-conjugated)	N/A	Vector Labs (FL-1201)	FC	1:100	Extracellular (unfixed)
NG2 Chondroitin Sulfate Proteoglycan	Rabbit	Millipore (AB 5320)	IF/FC	1:200 (IF)/1:50 (FC)	Intracellular (fixed)
Pax6	Rat (APC)	Miltenyi Biotec (130-107-829)	IF/FC	1:100 (IF)/1:50 (FC)	Intracellular (fixed)
PDGFRa	Rat (APC)	Biolegend (APA5)	IF/FC	1:100 (IF)/1:50 (FC)	Extracellular (unfixed)
PKCa	Rabbit	Santa Cruz (H-7)	IF/FC	1:200 (IF)/1:50 (FC)	Intracellular (fixed)

Secondary antibody	Antibody species	Supplier	Application	Dilution
AF633-conjugated secondary antibodies	Goat	Thermo Fisher Scientific (A21052; A21070; S21375)	IF/FC	1:500 (IF)/1:200 (FC)
Biotin-conjugated secondary antibodies	Goat	Thermo Fisher Scientific (31430; 31460)	WB	1:2000 - 1:5000
Biotin-conjugated secondary antibodies	Rabbit	Dako (P0449)	WB	1:2000

Supplemental Table S3: List of antibodies and conditions used.

List of antibodies, dilutions and fixation used for immunofluorescence (IF), western blotting (WB) and flow cytometry (FC).

Target gene	Forward primer (5'-3')	Reverse primer (5'-3')	Probe (Roche Diagnostics)
Actb	aaggccaaccgtgaaaagat	gtggtacgaccagaggcatac	56
Cre	caataccggagatcatgcaa	cactatccaggttacggatatagttca	83
Dll1	aggggagctacacatgttcc	gggctaggagcacactcatc	11
Dll4	tactgctgctggcggtact	gctggttgacgaactcctg	11
Epo	tctgcgacagtcgagttctg	cttctgcacaacccatcgt	16
Hes1	tgccagctgatataatggagaa	ccatgataggctttgatgacttt	83
Hey1	acgacatcgtcccaggttt	actgttattgattcggtctcgtc	72
Hif1a	tgagcttgctcatcagttgc	cataacagaagctttatcaagatgtga	60
Hif2a	tgacagctgacaaggagaaaaa	caactcatagaagacctccgtctc	12
Notch 1	tggacgacaatcagaacgag	cctcaaaccggaacttcttg	85
Notch 4	ccatccagctgatgactcct	atccctgcaccagtgtcct	16
Pecam-1	cggtgttcagcgagatcc	actcgacaggatggaaatcac	45
Vegf (all isoforms)	actggaccctggctttactg	tgggacttctgctctccttc	64

Supplemental Table S4: real-time quantitative PCR primers and probes.

List of primers and probes (Roche Diagnostics, UK) used.

References

Grossman, R., Fox, L. E., Gorovits, R., Ben-Dror, I., Reisfeld, S. and Vardimon, L. (1994). Molecular basis for differential expression of glutamine synthetase in retina glia and neurons. *Mol. Brain Res.* **21**, 312–320.

Hitchcock, P., Macdonald, R., VanDeRyt, J. and Wilson, S. (1996). Antibodies against Pax6 immunostain amacrine and ganglion cells and neuronal progenitors, but not rod precursors, in the normal and regenerating retina of the goldfish. *J Neurobiol* **29**, 399–413.

Jeon, C.-J., Strettoi, E. and Masland, R. H. (1998). The major cell populations of the mouse retina. *J. Neurosci.* **18**, 8936–46.

Koso, H., Minami, C., Tabata, Y., Inoue, M., Sasaki, E., Satoh, S. and Watanabe, S. (2009). CD73, a novel cell surface antigen that characterizes retinal photoreceptor precursor cells. *Investig. Ophthalmol. Vis. Sci.* **50**, 5411–5418.

Liu, H., Kim, S.-Y., Fu, Y., Wu, X., Ng, L., Swaroop, A. and Forrest, D. (2013). An isoform of retinoid-related orphan receptor β directs differentiation of retinal amacrine and horizontal interneurons. *Nat. Commun.* **4**, 1813.

Liyanage, S. E., Fantin, A., Villacampa, P., Lange, C. A., Denti, L., Cristante, E., Smith, A. J., Ali, R. R., Luhmann, U. F., Bainbridge, J. W., et al. (2016). Myeloid-Derived Vascular Endothelial Growth Factor and Hypoxia-Inducible Factor Are Dispensable for Ocular Neovascularization-Brief Report. *Arterioscler. Thromb. Vasc. Biol.* **36**,.

Macosko, E. Z., Basu, A., Satija, R., Nemesh, J., Shekhar, K., Goldman, M., Tirosh, I., Bialas, A. R., Kamitaki, N., Martersteck, E. M., et al. (2015). Highly parallel genome-wide expression profiling of individual cells using nanoliter droplets. *Cell* **161**, 1202–1214.

Ozerdem, U., Grako, K. A., Dahlin-Huppe, K., Monosov, E. and Stallcup, W. B. (2001). NG2 proteoglycan is expressed exclusively by mural cells during vascular morphogenesis. *Dev. Dyn.* **222**, 218–227.

Ruether, K., Feigenspan, A., Pirngruber, J., Leitges, M., Baehr, W. and Strauss, O. (2010). Pkc-a is essential for the proper activation and termination of rod bipolar cell response. *Investig. Ophthalmol. Vis. Sci.* **51**, 6051–6058.

Stanescu-Segall, D., Birke, K., Wenzel, A., Grimm, C., Orgul, S., Fischer, J. A., Born, W. and Hafezi, F. (2015). PAX6 Expression and Retinal Cell Death in a Transgenic Mouse Model for Acute Angle-Closure Glaucoma. *J. Glaucoma* **24**, 426–32.

Tao, C. and Zhang, X. (2014). Development of astrocytes in the vertebrate eye. *Dev. Dyn.* **243**, 1501–1510.